4

Vibrational Spectroscopy of Gas Phase Functional Molecules and Their Complexes Cooled in Supersonic Beams

Takayuki Ebata, Ryoji Kusaka and Yoshiya Inokuchi
Hiroshima University,
Japan

1. Introduction

Functional molecules and supramolecules are the assemble of molecules, which are bound by noncovalent interactions, such as dispersion force, coordinate-bonding, hydrogen-bonding, etc. They exhibit special functions by forming regular high dimensional structures controlled by those weak interactions. The concept of the supramolecule was first proposed by Jean-Marie Lehn, who succeeded in synthesizing cryptand (Lehn, 1995). In the early stage, many studies have been carried out for host-guest complexes of crown ether (Gokel, 1991; Izatt et al., 1969; Pedersen, 1967; Pedersen & Frensdorff, 1972), calixarene (Atwood et al., 2002; Gutsche, 1998; Purse et al., 2005; Thallapally et al., 2005), and cyclodextrin (Brocos et al., 2010; Szejtli, 1988). These studies are extended to larger size systems built by several units, such as protein, Langmuir- Blodgett (LB) film, self assembled monolayer (SAM), and liquid crystal. In addition, more complicated molecular assemblies, rotaxane, catenane, and molecular capsules, are synthesized. Also, many functional groups have been used to applications such as sensing and basic chemical research, by covalently linking fluorescent dyes, nanoparticles, proteins, DNA, and other compounds of interest. Biomolecules may also be categorized to the functional molecules. In the biomolecules, many units form high dimensional structure through noncovalent interactions and exhibit special functions which are not possible for each unit.

Among many experimental studies on the functional molecules, vibrational spectroscopy is one of the most general methods. By examining the frequency shift and intensity change of the specific vibrations sensitive to the local interaction, we can study which part or site of the molecule bound for the complexation. In this sense, it is necessary to investigate vibrational spectra not only of the complexes but also of each unit under the isolated condition. By the comparison of the spectra at different conditions, we understand how the molecules change their initial structures or which conformer is preferred for the complexation. A problem for this study is that in most cases they have flexible structures so that the structures are affected by many factors, such as temperature, local environment, solvent molecules as well as the phases. These effects result in the homogenous and inhomogeneous broadening of the spectra, which leads to the difficulty to analyze the spectra.

In this chapter, we describe the vibrational spectroscopic study of gas phase small size functional molecules cooled in the supersonic jet. The supersonic jet technique enables us to

cool the internal temperature of molecules and complexes. We apply several spectroscopic methods to these molecules. Laser induced fluorescence (LIF), one-photon resonant two-photon ionization (R2PI) and ultraviolet-ultraviolet hole burning (UV-UV HB) spectroscopic methods are used to obtain the S_1-S_0 electronic spectrum and discriminate different species, such as conformers and isomers. The infrared (IR) absorption spectrum is obtained by IR-UV double resonance (IR-UV DR) spectroscopy, which was developed to obtain the IR spectra of selected species with low concentration. IR photodissociation (IRPD) spectroscopy is another version of the IR spectroscopic measurement. By comparing the IR-UV DR and IRPD spectra, we can obtain the dissociation energy of the complex.

We first review our vibrational spectroscopic study on the conformation of *L*-phenylalanine (*L*-Phe) and *L*-tyrosine (*L*-Tyr), and the structure of the hydrated complexes. We show the discrimination of different conformers by IR-UV DR spectroscopy and how the initial geometry changes when they form complexes with water molecules. We then review the study on the encapsulation complexes of dibenzo-18-crown-6-ether (DB18C6), benzo-18-crown-6-ether (B18C6), calix[4]arene (C4A). For crown ethers (CEs), we first examine the possible conformations in bare form and then investigate how the CEs change their conformation to encapsulate the guest species in their cavities. We also comment on the molecular recognition in the process of the encapsulation. For C4A, we investigate encapsulation complexes with variety of guest species to extract which noncovalent interaction is the major component to encapsulate each guest species.

For the determination of the conformation as well as the complex structures, high level quantum chemical calculations play the important role, which provide the probable structures and the prediction of their IR spectra. Throughout this chapter, we use this experimental and theoretical joint approach to analyze the UV and IR spectra, leading to the determination of the structure of the supramolecules

2. Experimental methods

Figure 1(a) shows the experimental setup of the supersonic beam and laser system. The supersonic jet of the functional molecules is generated by an adiabatic expansion of the gaseous mixture of the sample (host functional molecule) and guest species into the vacuum chamber. The adiabatic expansion generates internally cold gaseous molecules and complexes, with most of them populated in the zero-point vibrational level. However, the cooling during the expansion occurs under non-equilibrium conditions so that several conformers may coexist in the jet. We used a home-built high temperature pulsed nozzle (inset) to generate jet-cooled amino acids, CEs, C4A and their complexes with guest molecules. The pulsed nozzle consists of a commercially available solenoid valve and a sample housing made of polyimide resin. The sample housing which contains sample powder is attached to the head of the commercially available pulse valve and the housing is heated to 140-160 °C to evaporate the samples (Ebata, 2009). The housing has a 1mm orifice at the exit. The opening of the poppet located in the pulse valve is controlled externally to inject the sample gas, which is synchronized with the pulsed lasers. The gaseous mixture of the sample and guest species, premixed with helium or neon carrier gas at a total pressure of 2 bar, is expanded into the vacuum chamber through the orifice. The molecules are internally cooled (T_{rot} = ~10 K) by an adiabatic expansion, and we obtain supersonic free jet. By introducing a skimmer at the downstream of the free jet, a supersonic beam is obtained.

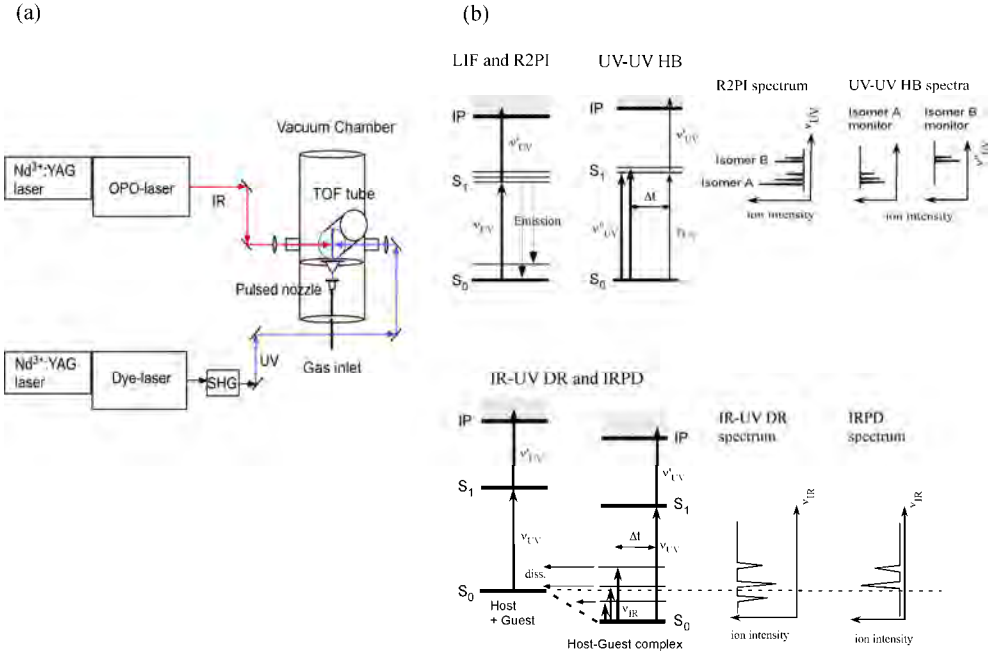

Fig. 1. (a) Experimental setup of the supersonic beam and IR-UV DR spectroscopy. (b) Laser spectroscopic methods used: (upper trace) UV spectroscopy and (lower trace) IR spectroscopy.

We apply several laser spectroscopic methods to obtain the electronic and vibrational spectra of the species generated in the supersonic jet. For the measurement of the electronic spectrum we apply LIF and mass-resolved R2PI [left panel of Figure 1(b)] spectroscopy. For the measurement of LIF spectrum, a tunable nanosecond UV laser pulse crosses the free jet at 20 mm downstream of the nozzle and excites the jet-cooled molecules to the upper electronic state (S_1). The florescence emitted from the molecules is monitored with a photomultiplier tube. By scanning the UV laser frequency while monitoring the total florescence, an LIF spectrum corresponding to the S_1-S_0 spectrum is obtained. For the R2PI measurement, the UV laser ionizes the molecules by one-photon resonant two-photon ionization scheme via the S_1 state. The generated ions are mass-separated by time-of-flight (TOF) tube and detected by a channeltron. The S_1-S_0 UV spectrum is obtained by scanning the UV frequency while monitoring the mass selected ions by a channeltron detector.
The discrimination of the different species in the electronic spectra is carried out by UV-UV HB spectroscopy [right panel of Figure 1(b)] (Ebata, 1998). In this method, two UV laser beams, namely "pump" and "probe" beams, are used. The pump laser pulse crosses the jet at 10 mm downstream of the nozzle, and the probe laser pulse crosses the jet 20 mm downstream of the nozzle. Here, the pump laser light is introduced ~ 4 μs prior to the probe laser light, corresponding to the 10 mm distance of the jet. The frequency of the probe UV laser is fixed to a band of a specific species and that of the pump UV laser is scanned. When the pump laser frequency is resonant to a transition of the monitored species, these species is excited to the upper state resulting in the depletion of the fluorescence or the ion signal

monitored by the probe laser light. Thus, the electronic spectrum of the monitored species is obtained as a function of the pump UV frequency.
For the measurement of the IR spectrum of a specific complex we apply IR-UV DR spectroscopy [lower panel of Figure 1(b)] (Brutschy, 2000; Ebata, 2009; Ebata et al., 1998; Tanabe et al., 1993; Zwier, 1996). The principle of this technique is very similar to UV-UV HB spectroscopy, except we use a tunable IR laser light for the pump laser. The IR and UV laser lights are spatially overlapped in the vacuum chamber. The IR laser is introduced ~100 ns prior to the probe UV laser light and its frequency is scanned. Depletion of the monitored signal occurs when the IR frequency is resonant to a vibrational transition of the monitored species and the IR spectrum is obtained as a depletion spectrum. For the complexes of C4A we apply IR photodissociation (IRPD) spectroscopy for obtaining the binding energy [lower panel of Figure 1(b)] (Hontama et al., 2010). In IRPD spectroscopy, the probe UV frequency is fixed to the electronic transition of C4A. When the absorbed IR energy is larger than the binding energy of the C4A complex, the complex dissociates to produce the C4A fragment. Thus, by scanning the IR frequency while monitoring C4A fragment, we obtain the IRPD spectrum. By comparing IRPD and IR-UV DR spectra, we obtain the threshold to generate the C4A fragment which is equal to the binding energy of the complex.

3. Theoretical methods

As was described in the introduction, quantum chemical calculation plays an important role to determine the structures of functional molecules as well as the binding energies. Most of the calculations are carried out by density functional theory (DFT) calculations with the B3LYP or M05-2X functional and the 6-31+G* basis set using the GAUSSIAN 09 program package (Frisch et al., 2009). For the complexes of C4A, in addition to the DFT calculation, a higher level quantum chemical calculation is performed to optimize the structures and obtain accurate binding energies of the complexes. These include the second order Moller-Plesset (MP2) level of theory (Møller & Plesset, 1934) and the family of augmented correlation consistent basis sets of Dunning and co-workers (Dunning, 1989; Kendall et al., 1992) up to quadruple-zeta quality, aug-cc-pV*n*Z (*n* = D, T, Q). The MP2/aug-cc-pVDZ optimal geometries were used for single point calculations with the larger basis sets up to aug-cc-pVQZ. For the detail of the calculation, see ref. (Hontama et al., 2010).
The energies of the optimized structures were corrected by zero-point vibrational energy. The harmonic vibrational frequencies were scaled by the factors of 0.97 and 0.95 for the OH and CH stretching vibrations, respectively, in order to compare with the experimentally measured ones. The S_1–S_0 electronic transition energies were calculated using time dependent density functional theory (TD-DFT) with the same functional and basis set.

4. Conformation and hydrated structures of amino acids

4.1 L-Phenylalanine (L-Phe)

The three-dimensional structures of peptides and proteins and their dynamics are to a large extent governed by the conformational profiles of amino acids constituting them. In particular, competition between intra- and inter-molecular hydrogen-bonded interactions plays a vital role in determining the structure of the proteins in solution. In this section, we investigate the conformation of amino acids in bare form and the structures of the hydrated complexes. The conformational landscape of isolated *L*-Phenylalanine(*L*-Phe) (Scheme 1) has

been examined in detail by several groups (Ebata et al., 2006; Hashimoto et al., 2006; Robertson & Simons, 2001; Snoek et al., 2000; Von Helden et al., 2008). The key point of these studies is that different conformers and isomers exhibit different UV transition energies.

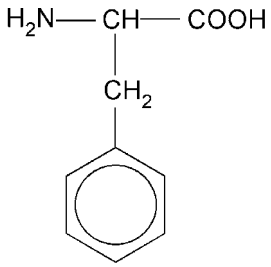

Scheme 1. L-Phenyl alanine

Figure 2(a) shows the LIF and R2PI spectra of jet-cooled *L*-Phe in the origin region of the S_1-S_0 transition. The inset shows the UV absorption spectrum of *L*-Phe in solution. There are several peaks in the band origin region, and Figure 2(b) shows the IR-UV DR spectra obtained by monitoring the marked bands (**A, B, C, D, E** and **X**) in the LIF spectrum. Other peaks are assigned to the vibronic bands of these conformers (Snoek et al., 2000). The labeling for each band is adopted from Ref. (Snoek et al., 2000). As seen in Figure. 2(b), their IR spectra are different from each other, and it is concluded that there are at least six conformers of *L*-Phe in the jet. The conformers **A, C, D,** and **E,** have the free OH stretching vibration of carboxyl OH group at ~3590 cm^{-1}, while the conformers **B** and **X** exhibit largely red-shifted OH stretch at 3280 and 3240 cm^{-1}, respectively. These large red-shifts are due to the intramolecular hydrogen(H)-bonding between the carboxyl OH and the amine nitrogen. The stick diagrams in Figure 2(b) are the calculated IR spectra for the possible conformers for the species **A, B, C, D, E** and **X,** whose structures are shown in Figure 3. In the figure, the number in the parentheses are the zero-point-energy corrected relative energy (kJ/mol) obtained at MP2/6-31+G* level (Ebata et al., 2006).

The structural information gives the conformer dependent photo-physics of *L*-Phe. By comparing the relative band intensities between the LIF and the R2PI spectra, it is obvious that the relative intensities are quite different between them. Especially the intensity of band **X** is quite weak in the LIF spectrum compared to other bands, while its intensity is comparable to other bands in the R2P1 spectrum. The LIF intensity is proportional to the product of the S_1-S_0 absorption cross section and the fluorescence quantum yield, while the R2PI band intensity is roughly proportional to the absorption cross section. Thus, it is suggested that fluorescence quantum yield of the species associated to band **X** is much smaller than other conformers. Actually, the florescence lifetime of the species **X** is 29 ns, while those of other conformers are 70~90 ns (Hashimoto et al., 2006). Thus, it is concluded that S_1 lifetime of *L*-Phe is quite different for different conformer even in the bare molecule. The short lifetime of conformer **X** having the intramolecular H-bonding may be ascribed by the fast internal conversion or intersystem crossing to the nearby $n\pi^*$ state.

As was described above, there are at least six conformers in the jet, which are classified to the intramolecular H-bonded group and to the non-H-bonded groups. In this section, we investigate how *L*-Phe changes its conformation to form the complex with water molecules. Figure 4 shows the LIF spectrum of jet-cooled *L*-Phe measured under different partial pressure

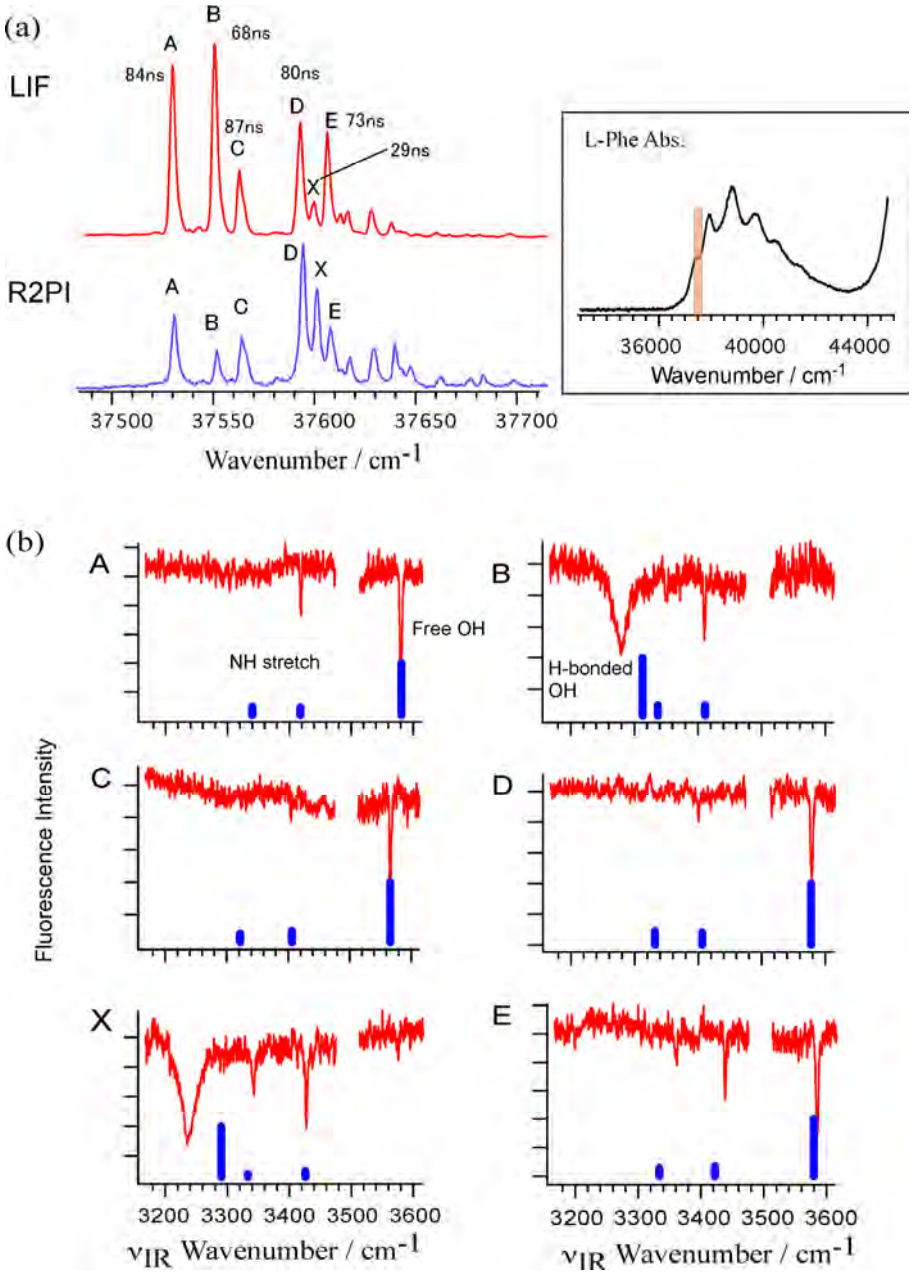

Fig. 2. (a) LIF and R2PI spectra of jet-cooled *L*-Phe. (b) IR-UV double resonance spectra of *L*-Phe for the bands marked in the LIF spectrum. Stick diagrams are the calculated IR spectrum of the corresponding conformers shown in Figure. 3. Inset is the UV absorption spectrum of *L*-Phe in solution. Figure adapted from Ref. (Ebata, 2009).

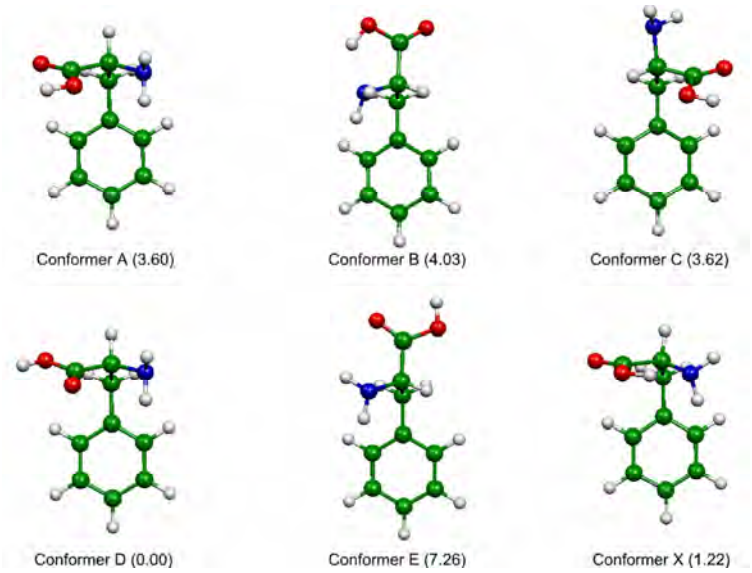

Fig. 3. Optimized structures of *L*-Phe at the MP2/6-31+G* level. Figure adapted from Ref. (Ebata et al., 2006).

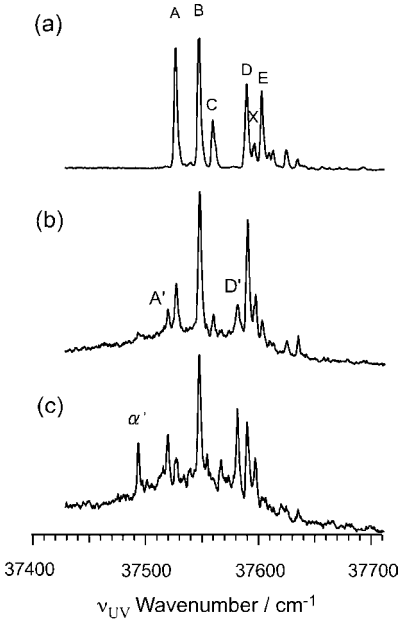

Fig. 4. LIF spectrum of jet-cooled *L*-Phe and *L*-Phe-$(H_2O)_n$ obtained under different water vapor pressure condition; (a) without water vapor. (b) water vapor at 0 °C. (c) water vapor at room temperature. He gas at a total pressure of 2.5 bar was used as a carrier gas. Figure adapted from (ref. Ebata et al., 2006)

of water vapor in the He expansion (Ebata et al., 2006). Here, the partial pressure of water vapor increases in the order from (a) to (c). The spectra of Figures 4(b) and (c) are measured at higher sensitivity than that of Figures 4(b), and are normalized by the intensity of band **B**. As seen in Figures 4(b) and (c), the band intensities of the conformers **A, D** and **E** become weaker than the band **B**, and new bands, **A′, D′**, and **α′** appear at 37520, 37582 and 37492 cm^{-1}, respectively. The conformers **A, D** and **E** are the non-H-bonded open conformers and it is seen that water molecules easily form H-bonding to the open-type conformers. On the other hand, it seems difficult for the water molecules to be incorporated in the closed conformer by breaking the intramolecular H-bond. The band **A′, D′** and **α′** were assigned to *L*-Phe-$(H_2O)_{1,2}$ by mass-selected two-color R2PI measurement (Lee et al., 2002), though their structures were not revealed at that time. It is clear that IR-UV DR spectroscopy unambiguously revealed their structures.

The IR-UV DR spectra observed by fixing UV frequencies to bands **A′, D′** and **α′** are shown in the upper panel of Figures 5(a)-(c). In the IR-UV DR spectrum of band **A′**, which is assigned to *L*-Phe-$(H_2O)_1$, there are two intense bands at 3246 and 3506 cm^{-1}, and three sharp bands at 3040, 3421 and 3724 cm^{-1}. Though it is *a priori* not clear whether *L*-Phe retains a similar conformation under the formation of the H-bonding with water, it is reasonable to assume that the isomer **A′** has the *L*-Phe conformation similar to conformer **A**, because the intensity of band **A′** increases parallel to the decrease of band **A**, and the small red-shift in the electronic transition of band **A′** with respect to band **A** (7 cm^{-1}) is also observed in other monohydrated aromatic acids. Thus, the structures of *L*-Phe-$(H_2O)_1$ were calculated with *L*-Phe part forming conformer A. Three H-bonding sites are possible for *L*-Phe; the carboxyl group, the amino group and the phenyl group. Among them, it was found that the H-bonding to the carboxyl group results in the most stable isomer, and the calculated IR spectrum reproduces very well the observed one. Figure 5(a) also shows the most stable isomer (Aw1-I) and the calculated IR spectrum as a stick diagram. In this isomer, the water forms a cyclic H-bond with the carboxyl group. The intense and broad bands at 3246 and 3506 cm^{-1} are the H-bonded carboxyl OH and the water donor OH stretch bands, respectively, within the cyclic H-bonding network. The sharp bands at 3421 and 3724 cm^{-1} are assigned to the asymmetric NH_2 stretch of amino group and free OH stretch of water, respectively. The IR spectrum of band **D′** (Figure 5(b)) is similar to that of band **A′**, because the red-shift of band **D′** from band **D** in the electronic transition, that is 8.5 cm^{-1}, is close to that of band **A′** from band **A**. Thus, the structure of *L*-Phe-$(H_2O)_1$ was calculated with *L*-Phe forming conformer **D**. It was found that the isomer in which the water molecule forms a cyclic H-bond with the carboxyl group (Dw1-I) is the most stable structure and the IR spectrum of Dw1-I well reproduces the observed one.

Upper panel of Figure 5(c) shows the IR spectrum obtained by fixing UV frequency to band **α′**. In the spectrum, a very broad and strong band is seen at 3002 cm^{-1}. Several sharp bands are overlapped with this broad band, which are assigned to the aromatic CH stretch. Other intense peaks are seen at 3330, 3474, 3680 and 3717 cm^{-1}. The two bands at 3680 and 3717 cm^{-1} can be easily assigned to the OH stretch of water molecules free from H-bonding, and the appearance of the two free OH stretch bands suggests species **α′** to be *L*-Phe-$(H_2O)_2$. From the band position in the LIF spectrum, *L*-Phe part of species **α′** is thought to have a conformation similar to those bands **A** and **A′**. The calculated possible structures of *L*-Phe-$(H_2O)_2$ (Aw2-I) and their IR spectra are shown in Figure 5(c). In this complex, two waters

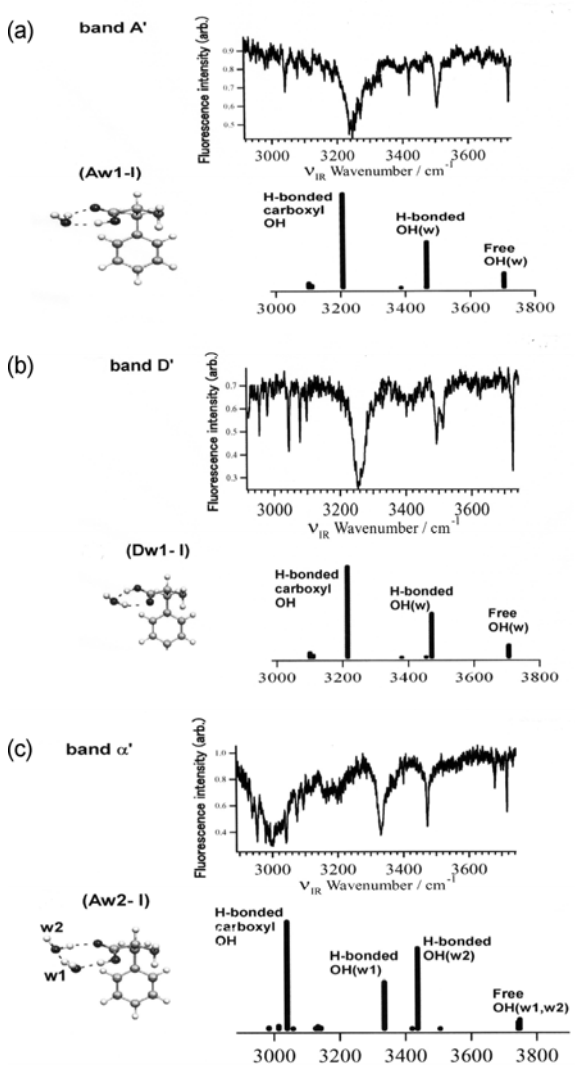

Fig. 5. IR-UV double resonance spectra of *L*-Phe-$(H_2O)_{n=1,2}$ by monitoring the bands marked in Fig. 4. Stick diagrams are the calculated IR spectra and the corresponding structures obtained at B3LYP/6-31+G* level. Figure adapted from (Ebata et al., 2006)

form cyclic H-bonding with a carboxyl group. A good agreement is seen between the calculated and observed IR spectra of Aw2-I. Thus, it is concluded that band **α'** is due to the cyclic-form *L*-Phe-$(H_2O)_2$ of Aw2-I. In Figure 5(c), the band at 3002 cm^{-1} is the H-bonded carboxyl OH stretch. Those at 3330, and 3474 cm^{-1} are the H-bonded OH stretches of two waters in the H-bond ring, and the bands at 3680 and 3717 cm^{-1} are OH stretches free from the H-bond. The weak and broad bands at ~3200 cm^{-1} are due to the overlapped transitions of the aromatic CH stretches. One noticeable point in the IR spectrum of *L*-Phe-$(H_2O)_2$ is that

the frequency shift of the carboxyl OH stretch with respect to bare *L*-Phe is as large as 580 cm^{-1}, which is more than twice the red-shift of the OH stretch of phenol-$(H_2O)_2$ (Watanabe et al., 1996), indicating that the carboxyl OH is considerably weakened under the hydration with two waters. This can be regarded as favorable for the proton transfer to take place in zwitter-ion formation.

4.2 L-tyrosine (L-Tyr)

L-Tyr is obtained by a substitution of the OH group at the para-position of *L*-Phe (Scheme 2). As seen in Figure 6, this substitution causes the number of possible conformers twice of *L*-Phe, arising from the difference of the direction of the OH group with respect to the main frame at the para-position. So, in the figure we label a number 1 or 2 for the classification of the conformers associated to the OH group. Figure 7 shows the LIF spectrum of jet-cooled *L*-Tyr (Inokuchi et al., 2007). The two spectra are obtained at different boxcar gate position to collect the fluorescence; (a) observed by monitoring the total fluorescence, (b) observed by

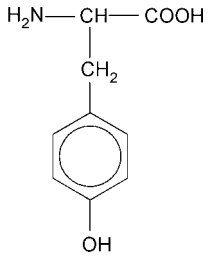

Scheme 2. L-Tyrosine

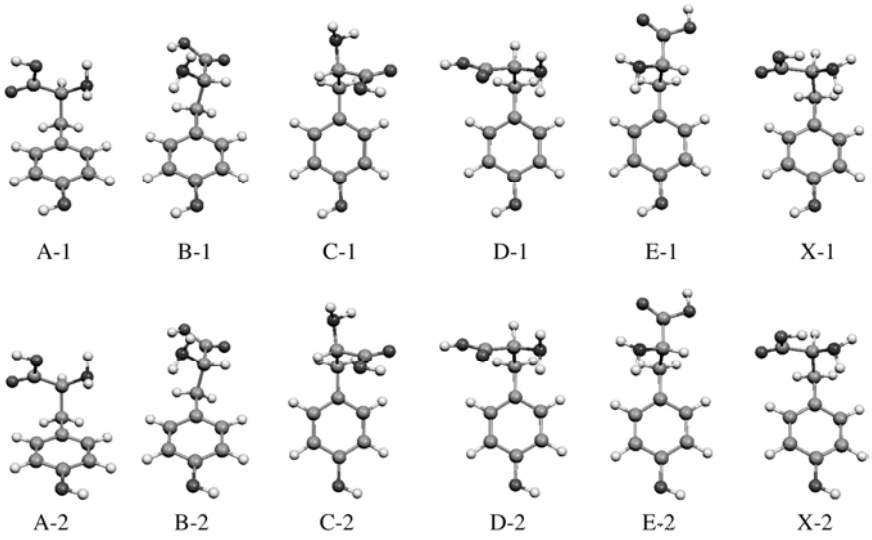

Fig. 6. Optimized structures of L-Tyr at the B3LYP/6-31+G* level. Figure adapted from Ref. (Inokuchi et al., 2007).

monitoring the florescence with the gate position of 12-27 ns after the laser excitation. The extra bands in Figure 7(a) which are not seen in Figure 7(b) are due to Tyramine which are generated by thermal decomposition of *L*-Tyr. The intensities of these bands increase with an increase of nozzle temperature. In the LIF spectrum, about 20 vibronic bands appeared in the 35450-35750 cm^{-1} region and the assignments of each bands are listed in Table 1.

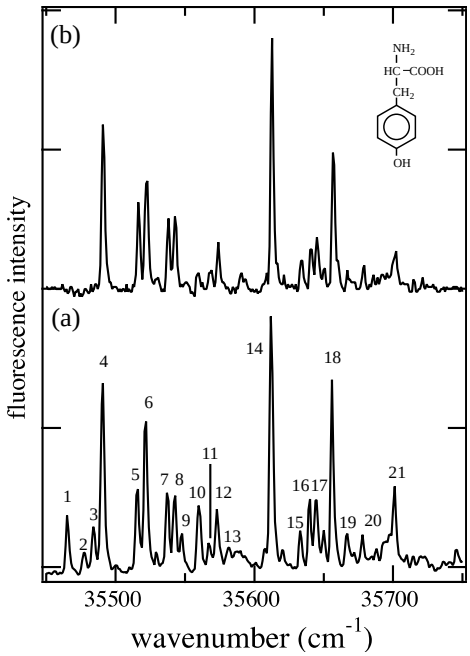

Fig. 7. LIF spectra of jet-cooled L-tyrosine measured with monitoring whole time window of fluorescence (a) and with monitoring a delayed gate position of 12–27 ns from the laser pulse (b). Figure adapted from Ref. (Inokuchi et al., 2007).

UV-UV HB spectroscopy has been applied to discriminate different conformers of *L*-Tyr, as shown in Figures 8 (Inokuchi et al., 2007). Left panel of the figure displays UV-UV HB spectra obtained by fixing the probe frequencies to bands **4**, **6**, and **14**, respectively. From these spectra, it is concluded that bands **4**, **8**, and **19** belong to the same conformer. Similarly, the HB spectra indicates that bands **6** and **12**, and a shoulder appearing on the lower frequency side of band **21** belong to the same conformer. The HB spectrum of Figure 8d indicates bands **14**, **18**, and **21** belong to the same species. By the same manner, the discrimination of all the bands can be carried out.

In addition to the discrimination of different species, the HB spectrum shows the features characteristic of the conformation of isomers in the low frequency (torsional) region. Right panel of Figure 8 shows the comparison of the UV-UV HB spectra for different conformers. The HB spectra show rich low frequency vibronic structure, and they can be classified into four groups (**k, l, m, n**) according to the spectral similarity. The HB spectra of bands **4** and **6** (Figures 8(a) and (b)) show three bands at 39, 52, and 177 cm^{-1} above the origin bands. We classify them into group **k**. The bands **5** and **7** (Figures 8c and 8d), exhibiting a weak band at 52 cm^{-1}, are classified into group **l**. The bands **16** and **17** (Figures 8e and 8f), showing two

Band	Position (cm^{-1})	Fluorescence Lifetime (ns)	Assignment[a]
1	35465	2.8	tyramine
2	35477	2.1	tyramine
3	35484	2.1	tyramine
4 (**k_1**)	35491	7.1	B
5 (**l_1**)	35516	5.0	**D**
6 (**k_2**)	35522	5.7	B′
7 (**l_2**)	35537	4.5	D′
8	35543	-	(B)
9	35548	2.4	tyramine
10	35560	2.5	tyramine
11	35567	-	-
12	35573	3.6	(B′)
13	35581	2.1	tyramine
14 (**m**)	35612	7.9	X, X′
15	35633	4.9	-
16 (**n_1**)	35640	4.1	E
17 (**n_2**)	35645	3.5	E′
18	35656	6.6	(X, X′)
19	35667	-	(B)
20	35678	-	-
21	35701	-	(X, X′)

Table 1. Band positions, lifetimes, assignments for vibronic bands in the LIF spectra of L-Tyrosine. [a]Assignments in parentheses show that these bands correlate with origin bands of corresponding conformers.

noticeable bands at 47 and 69 cm^{-1}, are classified into group **n**. The band **14** (Figure 8g) shows two bands at 44 and 89 cm^{-1}, and is classified into group **m**. The low frequency vibrations are assigned to the torsional modes of *L*-Tyr, such as torsion of the $HOOC(H_2N)CH$ group about the C_α–C_β bond, COOH torsion, and NH_2 torsion. These species belonging to each group are thought to have the very similar conformation of the main frame with each other.

Left panel of Figure 9 shows the comparison of the IR-UV spectra of bands **4**, **6** and **14** with B3LYP calculated ones of the conformers of **B-1** and **B-2** and **X-1** and **X-2** (Inokuchi et al., 2007). The bands **4** and **6** show very similar IR spectra with each other, while that of the band **14** shows the H-bonded OH stretch band at lower position and the asymmetric NH stretch at higher position than those of bands **4** and **6**. The calculated frequencies of the H-bonded OH band of **B-1** and **B-2** (3320 and 3319 cm^{-1}) are higher than those of **X-1** and **X-2** (3293 and 3297 cm^{-1}), and the asymmetric NH bands at 3475 and 3476 cm^{-1} of **B-1** and **B-2** are lower than those of **X-1** and **X-2** (3491 cm^{-1}). Thus, conformers belonging to bands **4** and **6** are assignable to **B-*n*** and band **14** to **X-*n***. The assignment of bands **4** and **6** to either of **B-1** or **B-2** is not possible at present, and they are labeled as **B** and **B′** (see Table 1). The conformer belonging to band **14** is assigned to " **X**, **X′** " in Table 1.

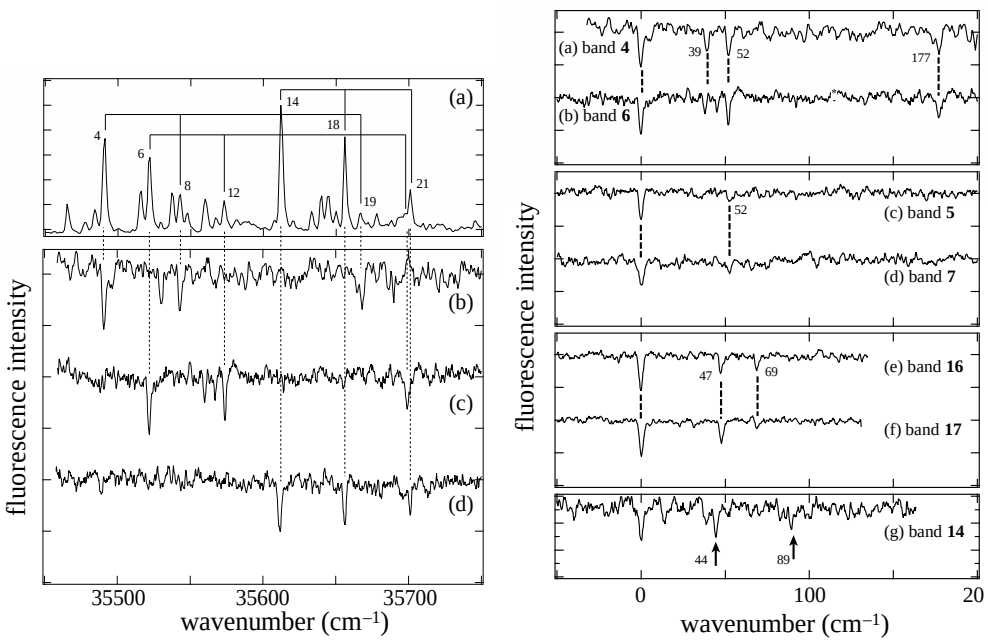

Fig. 8. (Left) Comparison of the (a) LIF spectrum and (b–d) UV-UV hole-burning spectra observed by probing bands **4**, **6**, and **14**. (Right) UV-UV hole-burning spectra for bands **4**, **6**, **5**, **7**, **16**, **17**, and **14**). The abscissa axis represents the energy relative to the transition energy of the origin bands. Figure adapted from Ref. (Inokuchi et al., 2007).

For other species (bands **5**, **7, 16** and **17**), their conformations can be determined based on the total energies and IR spectra. There are four candidates for them: conformers **A-*n*, C-*n*, D-*n*,** and **E-*n***. Among them, conformers **A-*n*** are excluded, because the calculated energies of **A-*n*** are much higher than other conformers at B3LYP level of calculation. Conformers **C-*n*, D-*n*,** and **E-*n*** have total energies similar with each other, and are assignable to bands **5, 7, 16** and **17** in terms of the total energy. As seen in Figure 6, only conformers **C-*n*** have a OH•••π hydrogen bond between the COOH group and the aromatic ring. A sign of the OH•••π hydrogen bond in conformers **C-*n*** emerges in IR spectra calculated. The right panel of Figure 9 shows comparison of the IR-UV DR for bands **5**, **7**, **16**, and **17** with calculated IR spectra for **D-*n*, E-*n*,** and **C-*n*** (Inokuchi et al., 2007). The OH stretching vibration of the COOH group of conformers **C-*n*** is calculated to be 3569 cm^{-1}, which is lower than those of conformers **D-*n*** and **E-*n*** (3582 and 3583 cm^{-1}, respectively). In the IR-UV DR spectra of *L*-Tyr, bands **5**, **7**, and bands **16**, **17** exhibit the OH stretching band of the COOH group around 3582 cm^{-1}, indicating that these groups do not have any hydrogen bond like the OH•••π bond. Therefore, possible structures for these species are conformers **D-*n*** and **E-*n*.** This result is supported by the experimental results of *L*-Phe; conformer **C** of *L*-Phe in Figure 2 has the carboxyl OH band at 3567 cm^{-1}, which is lower than those of conformer D (3579 cm^{-1}). For the assignment of groups **l** and **n** to conformers D-*n* or E-*n*, there is no unambiguous evidence for the assignment in the present stage. However, it is possible that group **l** is assigned to conformers D-*n*, and that group **n** is to **E-*n***, from the relative band intensities of the LIF spectrum and the calculated total

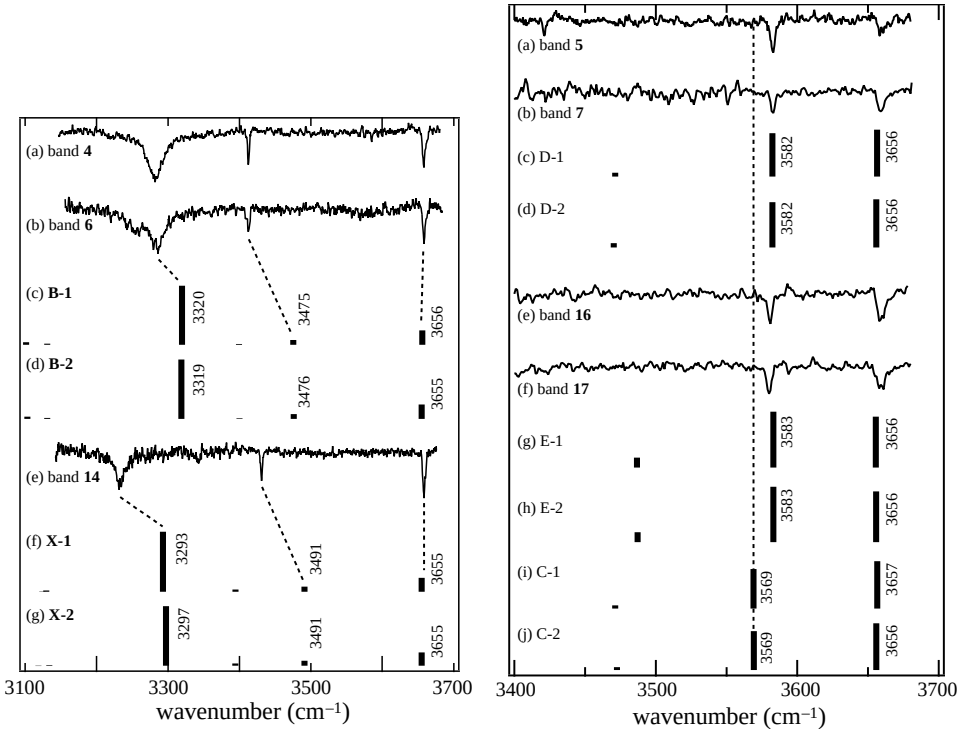

Fig. 9. (Left) IR-UV spectra observed at bands **4**, **6**, and **14** (a, b, and e). IR spectra calculated for conformers B-1, B-2, X-1, and X-2 (c, d, f, and g). (Right) IR-UV spectra observed at bands **5**, **7**, **16**, and **17** (a, b, e, and f). IR spectra calculated for conformers D-1, D-2, E-1, E-2, C-1, and C-2 (c, d, g–j). The dotted line is drawn at 3569 cm^{-1}. Figure adapted from Ref. (Inokuchi et al., 2007).

energies of the conformers. As seen in Figure. 7, bands of group **l** (bands **5** and **7**) are stronger than those of group **n** (bands **16** and **17**); the relative intensity is 1:0.75 between groups **l** and **n**. Assuming Boltzmann distribution at 363 K, which is the temperature of the sample source, and using the total energy calculated for conformers D-*n* and E-*n*, the relative population of conformers **D-*n*** and **E-*n*** is estimated at 1:0.65, comparable to the result derived from the band intensity. In addition, the order of the band position in the electronic spectra is **B, D, X,** and **E** from lower to higher frequency in the case of *L*-Phe. If this order is kept for *L*-Tyr, groups **l** and **n** correspond to conformers **D-*n*** and **E-*n*,** respectively.

The above studies on L-Phe and L-Tyr demonstrate the combination of supersonic jet-laser spectroscopic study (LIF, UV-UV HB and IR-UV DR) and the theoretical study is quite powerful to solve the complicated problems such as the determination of conformations of flexible molecules.

5. Encapsulation complexes of calix[4]arene

Calixarenes (CAs) are macrocyclic compounds that are well known in host-guest chemistry. Their structures are comprised of cavities that are formed by phenyl rings connected by

methylene and OH groups. The OH groups are strongly hydrogen-bonded with each other at the lower rim of the molecular cavity. This cavity functions as a molecular receptor and encapsulates variety of species through non-covalent interactions, forming various clathrates. The structures of the clathrates or complexes are normally studied by vibrational spectroscopy, NMR and X-ray diffraction methods at room temperature (Atwood et al., 1991; Benevelli et al., 1999; Kuzmicz et al., 2002; Molins et al., 1992). However, the thermal energy at room temperature is often equal to the host-guest interaction energy, especially for the complexes with neutral guest species. This yields very broad or complicated spectra arising from the contribution of possible conformers and fluctuation at the given temperature. The interaction with solvent molecules further affect the structure.

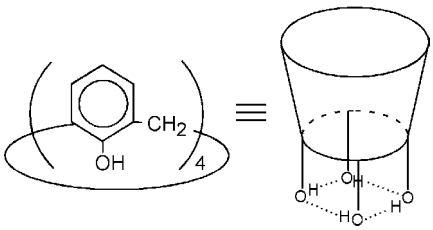

Scheme 3.Calix[4] arene (C4A)

Here, we carry out a supersonic beam-laser spectroscopic study for the complexes of calix[4]arene (C4A, Scheme 3), which is the smallest member of the CAs family. We investigate the structures of the complexes of C4A with variety of neutral guest species, namely Ar, CH_4, N_2, C_2H_2, H_2O, and NH_3 (Ebata et al., 2010; Hontama et al., 2010; Kaneko et al., 2011). These guests are chosen because they can be bound to the C4A host via different interactions, such as dispersion, XH-π hydrogen-bonding and dipole-dipole interactions. We examine how the different nature of the guest/host interaction affects the encapsulation structure, the electronic transition energy and the total binding energy.

Figures 10(a)-(g) show the S_1-S_0 LIF spectra of bare C4A and its complexes (Kaneko et al., 2011). The spectrum of bare C4A shows a sharp 0,0 band at 35357 cm^{-1}. In the higher region, several low frequency vibronic bands are observed. Especially, the vibronic bands at 35500 cm^{-1} region are stronger than the 0,0 band intensity. C4A has four identical chromophores, phenol, and under the C_4 symmetry their energies are split to ^1A, ^1B and ^1E by exciton coupling (Ebata et al., 2007). Among them, ^1A and ^1E are dipole allowed from the S_0 state. Thus, the band at 35357 cm^{-1} is assigned to the origin of the ^1A state and the intense bands at 35500 cm^{-1} are ascribed to the origin of the ^1E state or the vibronic bands appeared by the vibronic coupling between ^1A and ^1E.

The electronic transitions of all the complexes exhibit red-shift with respect to the bare molecule. The inset of Figure 10 shows the plot of the red-shift vs the polarizability of the guest species. For rare gas atoms as guests, a smooth relationship is obtained between the red-shift and the polarizability. Slight deviation for N_2, CH_4 and C_2H_2 from this relationship may be due to the anisotropy of their polarizabilities. For the complexes with H_2O and NH_3, the red-shifts are ~200 cm^{-1}, which is roughly 4 times larger than those of the complexes having the similar polarizabilities. Thus, the red-shift is quite dependent on the type of the guest species.

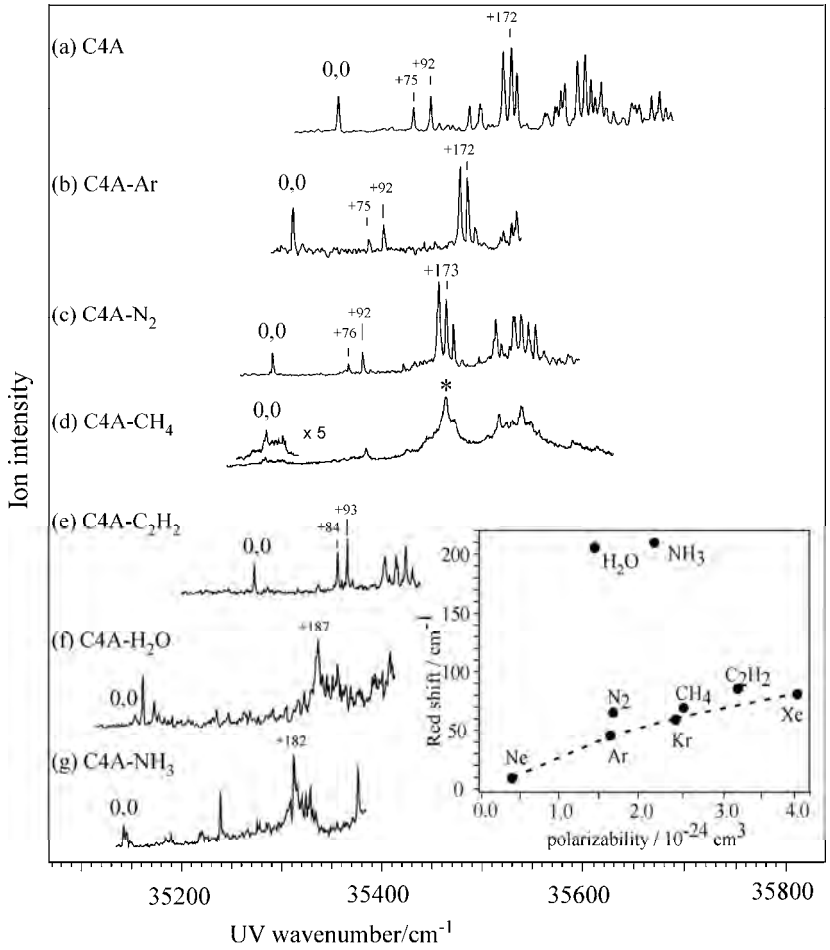

Fig. 10. R2PI spectra of (a) bare C4A and (b)-(g) its complexes. Inset shows the plot of the red-shifts of the complexes as a function of the polarizability of the guest species. Figure adapted from ref. (Kaneko et al., 2011).

Figures 11(a) shows the IR-UV DR spectra of bare C4A (Hontama et al., 2010). Figures 11(b) and (e) show the IR-UV DR and IRPD spectrum of C4A-H_2O. The IR spectrum of C4A exhibits a strong and broad OH stretching band centered at 3160 cm^{-1}. This band is red-shifted by ~500 cm^{-1} from the free OH stretch of phenol (3657 cm^{-1}). Thus, the four OH groups are strongly H-bonded with each other in C4A. The weak band at 3040 cm^{-1} is assigned to the CH stretching vibration of the aromatic ring. In the spectrum of the C4A-$(H_2O)_1$ complex, the broad H-bonded OH stretch band appears at the same frequency of bare C4A but its bandwidth is wider. The similarity of the OH stretching frequency between C4A-$(H_2O)_1$ and bare C4A indicates that the OH groups of C4A are not affected by the complexation with H_2O, that is the water molecule is not bound to the OH groups of C4A. In addition to the strong band at 3160 cm^{-1}, the IR-UV DR spectrum exhibits a weak band at

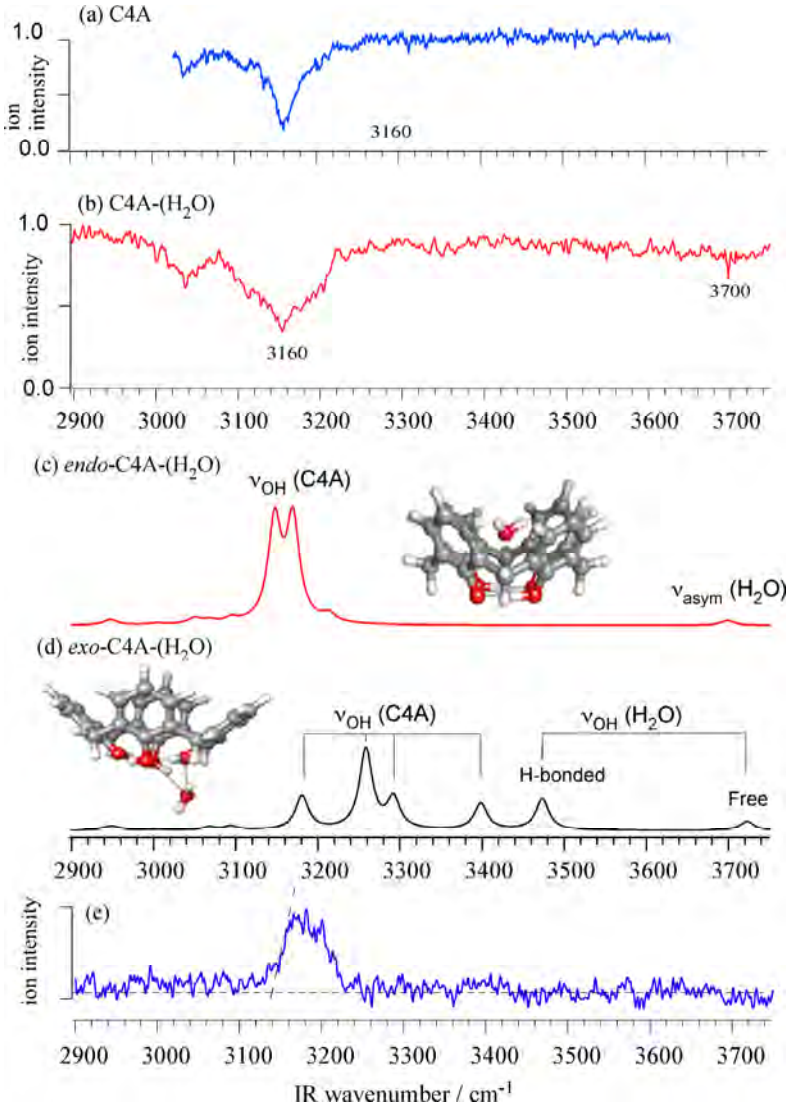

Fig. 11. IR-UV DR spectra of (a) C4A and (b) C4A-(H_2O). Optimized structures and IR spectra of (c) *endo*- (Structure II) and (d) *exo*-form of C4A-(H_2O) (Structure I) obtained at the MP2/aug-cc-pVDZ level of theory. (e) IRPD spectrum of C4A-(H_2O). Figure adapted from Ref.(Hontama et al., 2010).

3700 cm^{-1}, which is assigned to the anti-symmetric OH stretching vibration of the water molecule. This frequency is 56 cm^{-1} lower than that of gas phase water molecule so that the two OH groups of H_2O are H-bonded in the complex. Figure 11(e) shows the IRPD spectrum of C4A-$(H_2O)_1$. The spectrum is obtained by scanning the IR laser frequency while monitoring the $C4A^+$ signal with a UV frequency fixed near the band origin of C4A. When

we compare the IRPD and IR-UV DR spectra we see a sharp cutoff at 3140 $\pm$ 20 cm^{-1} in the IRPD spectrum, although the C4A-$(H_2O)_1$ complex shows the IR absorption in the IR-UV DR spectrum. Therefore this cut off means C4A-$(H_2O)_1$ does not dissociate below 3140 $\pm$ 20 cm^{-1} , corresponding to the C4A-$(H_2O)_1$ $\rightarrow$C4A + H_2O dissociation energy.

The optimal structures of the C4A-$(H_2O)_1$ complex is obtained at MP2/aug-cc-pVDZ levels of theory. The optimization predicts an *endo*-isomer structure, as a global minimum and a *exo*-conformer (Structure I) which are shown in Figures 11(c) and (d). In the *exo*-isomer (Structure I) the water molecule is inserted into and enlarges the ring H-bonding network originally formed by the four OH groups of C4A. The resulting five OH homodromic ring is consistent with the network having the largest cooperativity. In this structure, the H-bonding network of the OH groups in C4A is largely distorted by the insertion of the water molecule. As a result, the calculated IR spectrum of the *exo*-isomer (Structure I) predicts widely distributed OH stretching bands as shown in Figure 11(d). In contrast, the IR spectrum of the global minimum *endo*-isomer (Structure II) (Figure 11(c)) is much simpler, attesting to the minimal distortion of the C4A moiety in the C4A-$(H_2O)_1$ complex. This spectral pattern well reproduces the observed IR-UV DR spectrum of Figure 11(b). The degenerate OH stretching bands of C4A at 3160 cm^{-1} are slightly split into two due to the symmetry reduction since the encapsulation of the water molecule lowers the symmetry of C4A. This is the reason why the observed band at 3160 cm^{-1} is broader than that of bare C4A. The band at 3700 cm^{-1} is assigned to the anti-symmetric OH stretching vibration (ν_3) of the encapsulated water. In the *endo*-isomer (Structure II) the two OH groups of the water molecule are bound to two phenyl rings in a bidentate manner and the oxygen atom of the water molecule is facing towards the rim of C4A. This arrangement is thought to originate from the dipole-dipole interactions between C4A and the water molecule. The dipole moment of C4A is 2.37 Debye, oriented along the C_4 axis and pointing upward, and that of the water molecule is 1.855 Debye (Lide, 2001). Thus, the oxygen atom of the water molecule in the cavity prefers to be oriented towards the rim of C4A in order to maximize the dipole-dipole interaction between the two fragments. As was described, the asymmetric OH stretching frequency of the encapsulated water molecule is 56 cm^{-1} lower than that of gas phase water. This lower frequency shift indicates both the OH groups of the water in the cavity are bound to the phenyl group by the OH-π H-bonding. This synergy between the two OH-π H-bonding and dipole-dipole interactions results in the large stabilization energy of "Structure II" with respect to the H-bonded *exo*-isomer (Structure I).

The same synergy effect of the XH-π H-bonding and dipole-dipole interaction is expected for the C4A-$(NH_3)_1$ complex. Here the ammonia molecule has a dipole moment of 1.472 Debye (Lide, 2001). The two stable structures of the C4A-NH_3 complex corresponding to the *endo* and *exo* isomers are shown in Figure 12(a). In the *exo* complex, NH_3 is incorporated in the H-bonding network of the phenolic OH groups, while in the *endo* complex it is encapsulated inside the C4A cavity with the N atom directed to the lower rim. The *endo* complex is calculated to be 34.57 kJ/mol more sable than the *exo* complex at the MP2/aug-cc-pVDZ level. Figure 12(b) shows the comparison of the observed IR-UV DR spectrum with the calculated IR spectra of the two isomers. The calculated IR spectrum of the *endo* complex (Figure 12 (c)) exhibits an intense H-bonded OH band at 3160 cm^{-1}, while the *exo* complex has four distinct OH stretching bands (Figure 12 (d)). It is clear that the calculated IR spectrum of the *endo* isomer reproduces the observed IR spectrum. We can therefore conclude that the observed C4A-NH_3 complex also has the *endo* structure of Figure 13(a). The calculated dipole moments are 3.434 and 3.273 Debye for the C4A-H_2O and C4A-NH_3

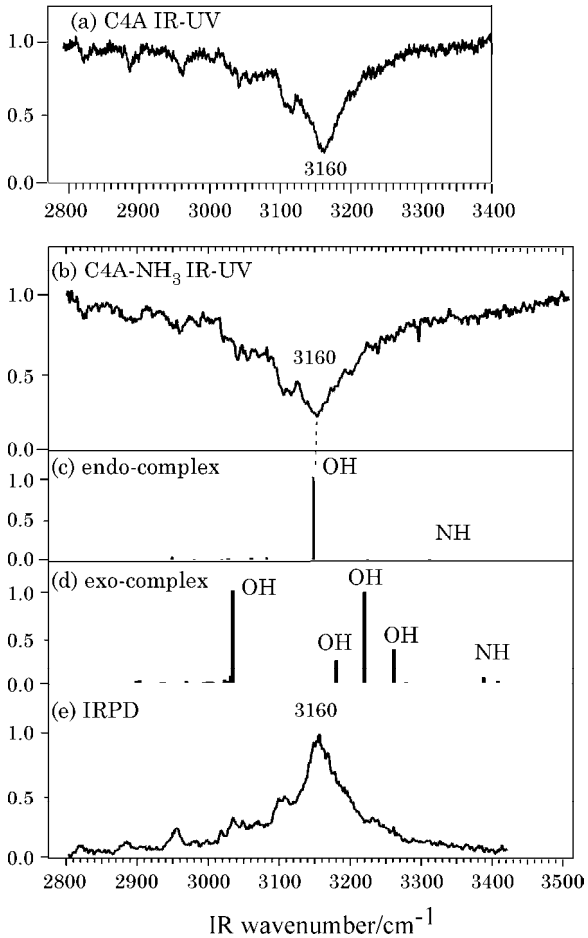

Fig. 12. a) IR-UV DR spectrum of C4A, (b) IR-UV DR spectrum of the C4A-NH_3 complex, (c)-(d) calculated IR spectra of the optimized structures of the *endo*- and *exo*- C4A-NH_3 complexes, (e) IRPD spectrum of C4A-NH_3. Figure adapted from ref. (Kaneko et al., 2011).

complexes, respectively. The binding energy for C4A-NH_3 is experimentally estimated to be less than 2810 cm^{-1}, which is slightly smaller than that of C4A-H_2O (3140 cm^{-1}), a difference that can be attributed to the smaller dipole moment of NH_3 when compared to H_2O as well as the smaller dipole moment of the C4A-NH_3 complex (3.273 D) when compared to that of the C4A-H_2O complex (3.434 D).

Figures 13(b)-(d) show the C4A complexes with N_2, CH_4, and C_2H_2 determined experimentally and by MP2/aug-cc-pVDZ level calculation (Kaneko et al., 2011). All the complexes are the *endo*-complex structure. For C4A-N_2 and -CH_4, they are bound by the dispersion interaction since the red-shifts of the S_1-S_0 transitions fall into the group of the C4A-rare gas complexes (Figure 10). In the C4A-N_2 complex, Figure 13 (b), N_2 is placed along the four-fold axis of C4A. The stability of this complex is due to the dipole-induced-dipole interaction between C4A and N_2. Because the overall C_4 symmetry is retained in the

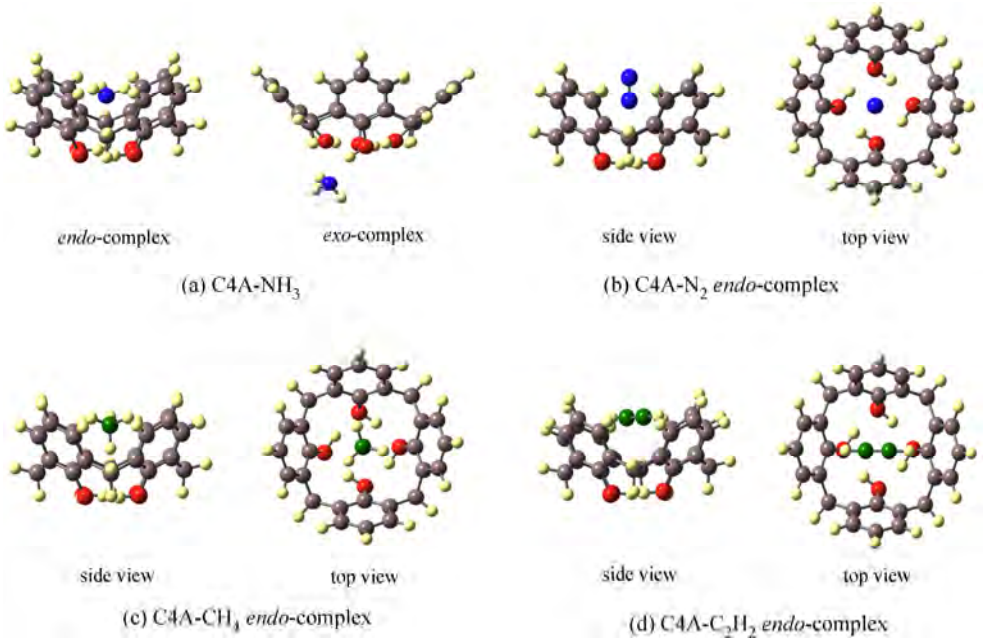

Fig. 13. The structures of (a) *endo*- and *exo*-complexes of C4A-NH_3, (b) *endo*- C4A-N_2 complex, (c) *endo*- C4A-CH_4 complex, and (d) *endo*- C4A- C_2H_2 complex. Figure adapted from ref. (Kaneko et al., 2011).

parallel isomer, the observed UV spectrum shows very similar features with that of the bare C4A. The structure of the *endo*-isomer of C4A-CH_4 is shown in Figure 13 (c). In this complex, one CH group is oriented along the 4-fold axis and points to the bottom of the C4A host. For the remaining three other CH groups, two are pointing towards the phenyl rings forming weak CH—π hydrogen bonding. In this arrangement, the OH stretching vibrations of the host C4A are unaffected by the complexation with CH_4. Indeed, the observed IR spectrum is very similar to that of bare C4A, a fact that is consistent with this structure. Since the complex does not retain the C_4 point group symmetry, the observed UV spectrum exhibits complicated structure. For the C4A-C_2H_2 *endo*-complex, Figure 13(d), C_2H_2 is located perpendicular to the four-fold axis of C4A so that the two CH groups form CH-π H-bonding with the phenyl groups. TheC4A host is distorted and the overall symmetry is reduced to C_2. This causes the degenerate OH stretching band of C4A to split into two bands, which is also identified in the observed IRPD spectrum.

6. Conformation and recognition of guest species of the crown ether complexes

Crown ethers (CEs) are cyclic ethers built with several oxyethylene (-C-C-O-) units (scheme 4). Applications of crown ethers as molecular receptors, metal cation extraction agents, fluoroionophores and phase transfer catalytic media have been described in a number of studies in the literature (Gokel, 1991; Izatt et al., 1969; Pedersen, 1967; Pedersen &

Frensdorff, 1972). One of the important aspects of the host/guest molecular systems is the selectivity in the encapsulation of guest species. There are two key factors controlling the selectivity: the size and the flexibility of the host cavity. First, if the cavity size of the host molecule fits the size of the guest species, the host shows an efficient selectivity for the encapsulation of the particular species. For example, in solution the 18-crown-6-ether (18C6) forms an exceptionally stable 1:1 complex with K^+ among alkali metal cations, because 18C6 forms a ring conformation of D_{3d} symmetry and the size of its cavity is comparable to the size of the spherical K^+. However, in the gas phase, 18C6 as well as 12-crown-4 (12C4) and 15-crown-5 (15C5) show the largest binding energy to Li^+ not to K^+ among the alkali-metal cations (Anderson et al., 2003; Armentrout, 1999; Glendening et al., 1994; More et al., 1999; Peiris et al., 1996). Very recently, it is reported that this largest binding energy of L^+-18C6 in the gas phase is due to the structure in which 18C6 can distort its ether frame to shorten the ether oxygen distance and maximize the biding energy (Inokuchi et al., 2011). Thus, the selectivity is substantially affected by the solvent molecules as well, and a stepwise study starting from the isolated molecule to micro-solvated complexes is essential. Molecular complexes provide an ideal environment for the precise study of the micro-solvated effects under solvent-controlled conditions. As was described above, the flexibility is the key point of crown ethers and they are able to adjust their conformations to fit the size and the shape of the guest species. We show how the structural flexibility affects the dynamics of the encapsulation for two CEs;dibenzo-18-crown-6-ether (DB18C6) and benzo-18-crown-6-ether (B18C6) and their complexes with various neutral molecules (Kusaka et al., 2007, 2008, 2009, 2011)

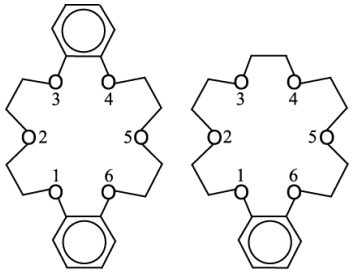

Scheme 4. Dibenzo-18-Crown-6 (DB18C6, left) and Benzo-18-Crown-6(B18C6, right)

6.1 DB18C6 and its complexes

Figure 14(a) shows the LIF spectrum of DB18C6 cooled in a supersonic jet (Kusaka et al., 2008). Figures 14 (b)-(h) show the UV-UV HB spectra measured by monitoring bands **m1**, **m2**, **a**, and **c-f**, respectively. From the UV-UV HB and mass selected R2PI measurements, it is confirmed that the bands **m1** and **m2** belong to the different conformers of DB18C6, and bands **a-f** to the DB18C6-$(H_2O)_{n=1-4}$ complexes. There are three noticeable points in the LIF spectrum. First for bare DB18C6, **m2** is the major species from the relative intensity. Second, all the hydrated complexes show blue-shifted band origins with respect to bare molecule. This means that DB18C6 plays the role of the acceptor of the H-bonding. Finally, the band origins of **m2** and **a** exhibit a 5 cm^{-1} splitting, which is descried as the exciton splitting of the two benzene chromophores in the same environment. In the LIF spectrum, the assignments of each bands are listed in Table 2.

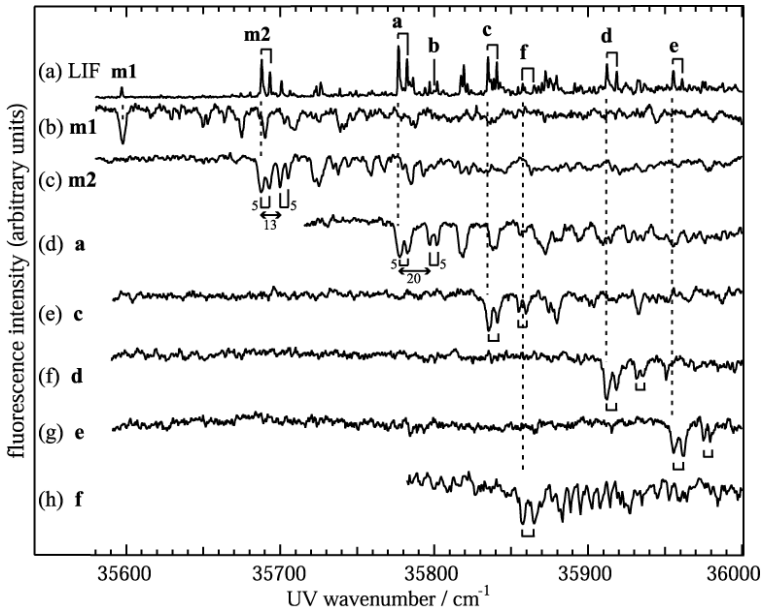

Fig. 14. (a) LIF spectrum of jet-cooled DB18C6 and its hydrated complexes. (b)-(h) UV-UV HB spectra measured by monitoring bands **m1**, **m2**, **a**, and **c**-**f** in the LIF spectrum, respectively. The numbers in (c) and (d) show the energy interval (cm^{-1}) in the corresponding regions. Figure adapted from Ref. (Kusaka et al., 2008).

Position / cm^{-1}	Label	Size	Assignment
35597	**m1**	DB18C6	IV
35688	**m2**		II
35777	**a**	DB18C6-$(H_2O)_1$	1W-1
35800	**b**		1W-2
35835	**c**	DB18C6-$(H_2O)_2$	2W-1
35858	**f**	DB18C6-$(H_2O)_4$	4W-2
35912	**d**	DB18C6-$(H_2O)_3$	3W-1
35955	**e**	DB18C6-$(H_2O)_4$	4W-1

Table 2. Band positions of origins for bare DB18C6 and the hydrated complexes (See Figure 16)

The IR-UV DR spectra in the CH stretching region for species **m1**, **m2**, and **a** are shown in Figure 15(b) (Kusaka et al., 2011). In the spectra, the bands in the 2800-3000 cm^{-1} region are the CH stretching vibrations of the methylene groups and those in the 3000-3100 cm^{-1} region to the CH stretching vibrations of benzene rings. In the methylene CH stretching region, the spectral patterns of **m1** and **m2** are similar with each other though they are the different

conformers. On the other hand, while species **a** shows a quite different spectrum. For example, **m1** and **m2** show a strong band at 2950 cm^{-1}, while species **a** does not. Instead, species **a** shows a strong band at 2830 cm^{-1} and weak one at 2800 cm^{-1}. Since IR spectra in the CH stretching region can reflect the conformation of crown ethers, the IR spectra in Figure 15(b) indicate that **m1** and **m2** have a structure similar with each other, while the DB18C6 conformation of species **a**, DB18C6-$(H_2O)_1$, is quite different from them.

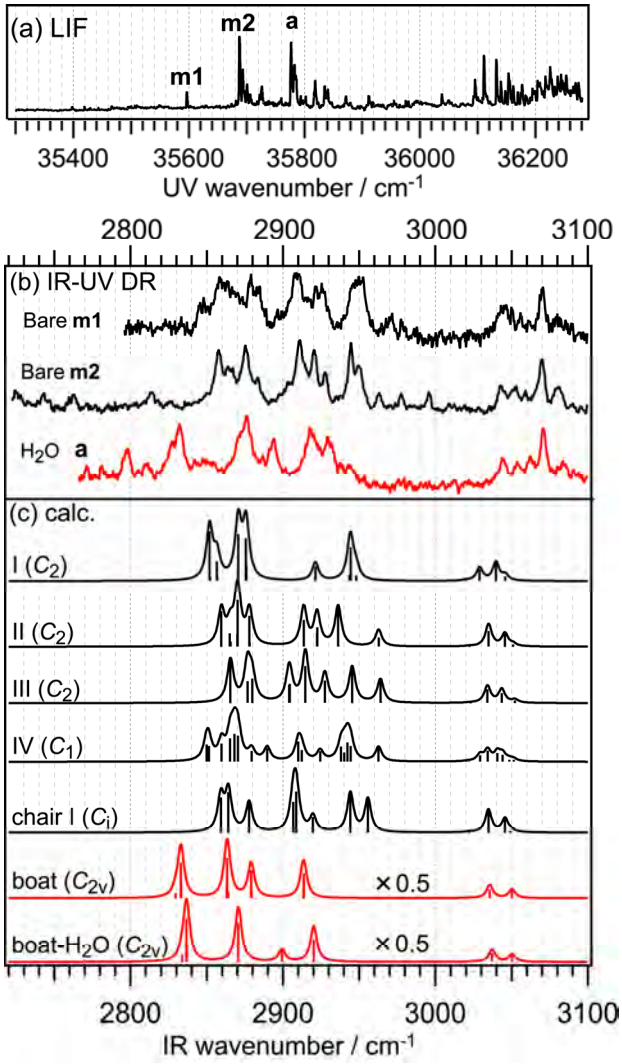

Fig. 15. (a) LIF spectrum of bare DB18C6 (**m1** and **m2**) and DB18C6-H_2O (species **a**). (b) IR-UV DR spectra of **m1**, **m2**, and **a**. (c) Calculated IR spectra of optimized bare DB18C6 and DB18C6-H_2O at M05-2X/6-31+G* level. The optimized geometries are shown in Figure 16. Figure adapted from Ref. (Kusaka et al., 2011).

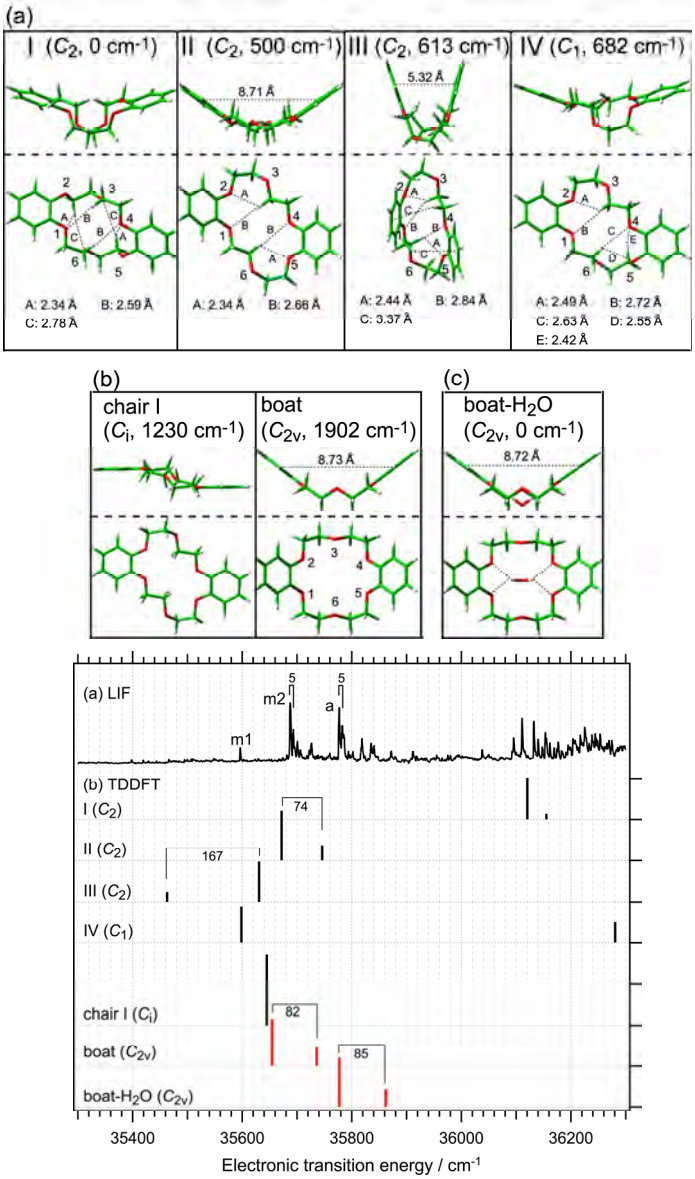

Fig. 16. (Upper) Optimized structures of bare DB18C6 and DB18C6-H_2O. (a) four most stable structures of bare DB18C6, (b) bare DB18C6 (chair I and boat), and (c) DB18C6-H_2O (boat-H_2O). Relative energies with respect to the most stable structure are displayed in cm^{-1} unit. The distances of CH$\cdots$O, CH$\cdots\pi$ and $\pi\cdots\pi$ are also indicated. (Lower) (a) LIF spectrum of bare DB18C6 and DB18C6-H_2O. (b) S_1-S_0 and S_2-S_0 electronic transition energies (bar graph) obtained by TDDFT calculations at the M05-2X/6-31+G* level. Figure adapted from Ref. (Kusaka et al., 2011).

The determination of the structures of **m1**, **m2**, and **a**, is carried out by the comparison of the observed IR spectra with the ones of the optimized structures obtained by quantum chemical calculations. Figure 16 shows the four most stable conformers of bare DB18C6 obtained at M05-2X/6-31+G* level (Kusaka et al., 2011). The energies (cm^{-1}) relative to the most stable conformer are displayed in the parentheses with the symmetry. In the figure, higher energy conformers; "chair I" and "boat" conformers, are also shown as the candidates for **m1** and **m2**. Figure 16 also shows the boat form DB18C6-$(H_2O)_1$, which is the most stable isomer of the 1:1 complex. In the structures in Figure 16, the crown frame of conformers **I**, **II**, **III**, and **IV** is fixed by the CH···O and π···π interactions, while such interactions seem very weak in the boat conformer.

Figure 15(c) shows the calculated IR spectra of the conformers of bare DB18C6 and boat-DB18C6-H_2O complex shown in Figure 16. The calculated IR spectrum of the boat conformer is quite different from those of the other conformers; it exhibits fewer IR bands than those of the other conformers because of its higher symmetry (C_{2v}). The calculated IR spectrum of boat DB18C6-H_2O well reproduces that of the boat conformer. The key for identifying the boat conformation is the appearance of bands at 2835 cm^{-1} and no band at ~ 2950 cm^{-1}. Thus, from the energetic and the similarity of the IR spectrum, it is concluded that the structure of species **a** is the boat-DB18C6-H_2O of Figure 16(c). We also see that the calculated IR spectrum of boat DB18C6-H_2O is very similar with bare boat DB18C6 as seen in the figure. On the other hand, the IR-UVDR spectra of species **m1** and **m2** (Figure 15 b) are quite different from that of the calculated boat DB18C6. Thus, the initial conformation of bare DB18C6 is not the boat form.

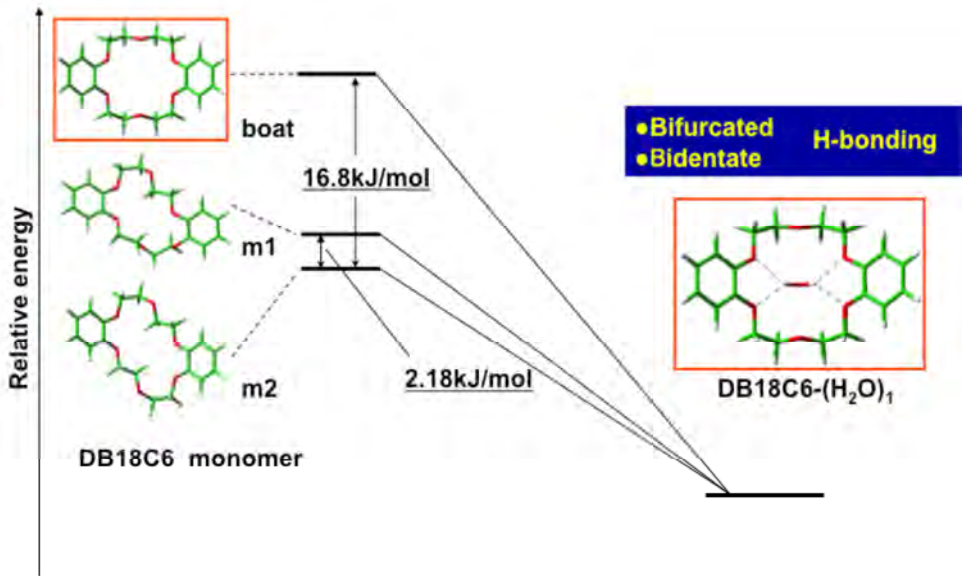

Fig. 17. Energetics of bare DB18C6 and DB18C6-H_2O obtained at the M05-2X/6-31+G* level. In bare DB18C6, the boat form is the higher energy conformer, while the boat conformer becomes the lowest energy conformer when it encapsulates a water molecule. In the complex, DB18C6 and H_2O are bound via bifurcated and bidentate hydrogen-bonding.

The determination of the structures of species **m1** and **m2** is carried out by the comparison of the observed IR and the electronic spectrum with the theoretically calculated ones. In the IR spectrum of the CH stretching region (Figure 15), we see that the spectra of conformers I-IV resemble each other and the observed IR spectra of species **m1** and **m2**. Thus, it is difficult to determine the structures from the IR spectra. So, we compared the electronic transition energies. Lower panel of Figure 16 shows the comparison of the LIF spectrum and the transitions of the different conformers of DB18C6 obtained by TD-DFT calculation. The calculated transition energies are scaled so that the energy of the boat DB18C6-H_2O fits to the observed band **a**. The split of ~80 cm^{-1} for conformers II and boat is due to the exciton splitting of DB18C6 in which the two chromophores are under the same environment of symmetry. Actually, the splitting is much smaller in the real molecules because the oscillator strength is spread to vibronic bands according to Franck-Condon principle. The observed splitting is 5 cm^{-1} for bands **m2** and **a**. This small exciton splitting indicates that band **m2** is due to the conformer II having the C_2 symmetry. The electronic transitions of other conformers are largely split due to the different environments of the chromophores. Among them, the positions of the conformers IV and Chair I are close to the band **m1**. Since conformer IV is lower energy conformer as shown in Figure 16, we conclude that band **m1** is due to the conformer IV.

The above results show that bare DB18C6 changes its conformer to the boat form to encapsulate the water molecule in this cavity, though the boat form is not the most stable structure in bare form shown in Figure 17. The boat conformation becomes most stable by the bidentate and the bifurcated hydrogen-bond formation. This conformation change is also found in the DB18C6-NH_3 complex, where the bidentate and the bifurcated hydrogen-bond is formed between the host DB18C6 and guest NH_3. On the other hand, when we use CH_3OH or C_2H_2 as a guest species such a conformation change does not occur since they can not form the bidentate and the bifurcated hydrogen-bonding. Thus, we can say that DB18C6 can recognize the difference of the guest species from the difference of the type of the H-bonding.

The hydrogen-bonded structures of DB18C6-$(H_2O)_n$ are revealed from the analysis of the IR-UV DR spectra in the OH stretching vibration, which are shown in the upper panel of Figure 18 (Kusaka et al., 2008). Figures 18(a) and (b) show the IR spectra for bands **a** and **b**, respectively, where the species of band **a** is the major species. From the appearance of two OH bands at different positions, they are due to different isomers of the DB18C6-$(H_2O)_1$ complex. The positions of the two vibrations are red shifted by 77 and 108 cm^{-1} for band **a** , and by 51 and 77 cm^{-1} for band **b** with respect to the vibrations of gas phase water, respectively. This is the evidence that in both complexes forms the bifurcated and bidentate H-bonding. Figure 18(c) shows the IR-UV DR spectrum of species **c**, corresponding to the DB18C6-$(H_2O)_2$ complex. The bands at 3562 and 3623 cm^{-1} are assigned to the symmetric and anti-symmetric OH stretching vibrations of a bidentate water molecule, respectively. Their positions are red shifted by 18 and 25 cm^{-1} from those of band **a**, meaning the O atom of the bidentate water acts as an acceptor for the second water molecule. The bands at 3401 and 3716 cm^{-1} can be assigned to the singly H-bonded and free OH stretching vibrations of the second water molecule, respectively. The IR-UV DR spectrum of band **d** in Figure 18(d) exhibits six OH stretching bands, suggesting this species is DB18C6-$(H_2O)_3$. In the spectrum the bands are located close to each other and no band appears at the free OH stretching region. Therefore all water molecules form bidentate H-bonds. The six bands are classified to three pairs of the symmetric and anti-symmetric OH stretching vibrations of the bidentate

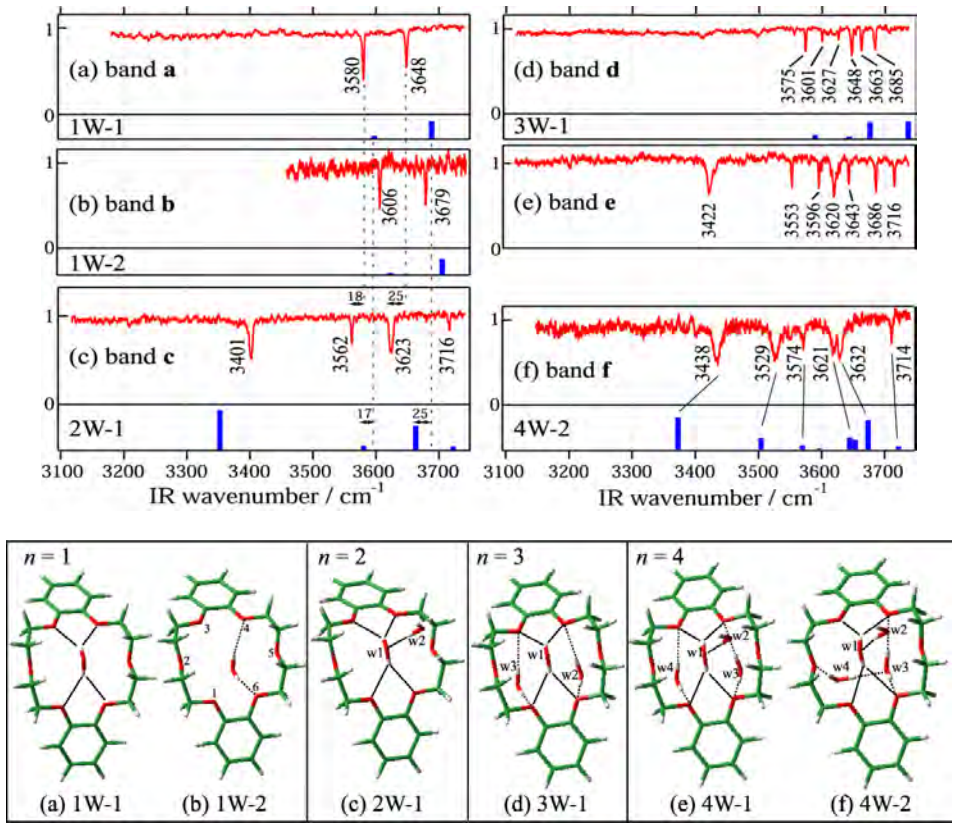

Fig. 18. (Upper) (a)-(f) IR-UV DR spectra of DB18C6-$(H_2O)_n$ measured by monitoring bands **a-f** in the LIF spectrum, respectively. Sticks under the IR-UV DR spectra denote the calculated IR spectra at the optimized structures. (Lower) Geometric features deduced from the analysis of the IR-UV DR spectra in the OH stretching region of species **a-f** of the DB18C6-$(H_2O)_n$ complexes. Figure adapted from Ref. (Kusaka et al., 2008).

water molecules. The lowest pair of the frequencies (3575 and 3648 cm^{-1}) is attributed to a bidentate water molecule bound to the bottom of the boat conformer and the other two pairs arise from the water molecules forming weaker bidentate H-bonds at the opposite (top) side of DB18C6. The spectrum of band **e** in Figure 18(e) shows seven bands and the band at 3620 cm^{-1} has a shoulder, indicating this species is DB18C6-$(H_2O)_4$. The 3422 and 3716 cm^{-1} bands can be assigned to the H-bonded and free OH stretching vibrations of a single-donor water molecule, respectively. The IR spectrum of species **e** in the 3550-3690 cm^{-1} region is very similar to species **d**. This suggests that the IR bands of species **e** can be assigned to the OH stretching bands of three water molecules H-bonded like those in 3W-1. The IR-UV DR spectrum of species **f** in Figure 18(f) indicates that this species is the isomer of DB18C6-$(H_2O)_4$. The 3438 cm^{-1} band can be assigned to the single-donor OH stretching vibration and the band at 3714 cm^{-1} is assigned to the free OH stretching vibration. The 3529 cm^{-1} band is unique to species **f**. This band is broad and is located on the lower frequency side of the

bidentate symmetric OH stretching vibration. Therefore, the 3529 cm^{-1} band cannot be assigned to a bidentate water H-bonded to the ether O atoms.
The lower panel of Figure 18 shows the most probable structures for species **a-f** obtained by DFT calculation and their predicted IR spectra are shown as blue bar graph. The two conformers, 1W-1 and 1W-2, of the DB18C6-$(H_2O)_1$ complex, correspond to species **a** and **b**, respectively. In both structures the conformation of DB18C6 is the boat form and the water molecule is H-bonded to the O atoms next to the benzene rings by bidentate H-bonding. However, in 1W-1, the water molecule is H-bonded to DB18C6 by the bifurcated and bidentate manner while in 1W-2 the two OH groups of the water are bonded directly to the O_4 and O_6 atoms, respectively. The OH stretching frequencies of 1W-1 are lower than those of 1W-2 due to the stronger hydrogen bonds. 2W-1 corresponds to species **c** (DB18C6-$(H_2O)_2$), in which the second water molecule (w2) is H-bonded to the O atom of the bidentate water molecule (w1). A noticeable feature of the spectra of species **c** is that the singly H-bonded OH stretching frequency (3401 cm^{-1}) is much lower than that of water molecules forming a normal H-bond. For example, the frequency of the donor OH stretching vibration in the water dimer is 3530 cm^{-1}. This large frequency reduction is due to that the O atom of the bidentate water molecule is highly negatively charged so that the second water molecule (w2) forms a strong H-bond.
3W-1corresponds to species **d** (DB18C6-$(H_2O)_3$). In this structure the first water molecule (w1) forms a bidentate H-bond at the bottom side of the boat DB18C6 like 1W-1 and the second (w2) and third (w3) water molecules form two bidentate H-bonds at the opposite side like 1W-2. The 4W-1 represents a hypothetical probable structure for species **e** (DB18C6-$(H_2O)_4$). This structure was not obtained as the stable form at the level of calculation used. 4W-2 shows a probable structure for species **f** (DB18C6-$(H_2O)_4$). In 4W-2, the first and second water molecules (w1 and w2) construct a bidentate and single-donor H-bonded network like 2W-I, whereas the third water molecule (w3) is bonded to the O_4 and O_6 atoms like 1W-2 and the fourth water molecule (w4) forms a bridge between an ether O atom (O_2) and the O atom of (w3). This type of H-bonding network was also found in the 18-crown-6-ether/water system at the liquid nitrogen temperature. The calculated IR spectrum for 4W-2 well predicts the band at ~3500 cm^{-1}, which is the stretching vibration of (w4) bonded to the O atom of (w3).

6.2 B18C6 and its complexes

Substitution of phenyl group(s) to CE makes the ether ring more rigid because the oxygen atoms adjacent to the benzene ring prefer the planar structure due to the delocalization of the π-electrons of benzene ring. In this sense, B18C6 is more flexible than DB18C6. We investigate how the difference in the flexibility affects its conformation as well as its complexation with water. Upper panel of Figure 19 shows LIF spectra of B16C6 in the band origin region observed without and with adding water vapor, respectively (Kusaka et al., 2009). Bands **M1-M4** and **A-I** are due to bare B18C6 and the B18C6-$(H_2O)_n$ complexes, respectively, because the addition of water vapor reduces the intensities of bands **M1-M4** and increases bands **A-I**.
Lower panel of Figure 19 show the observed IR-UV DR spectra for bands **A-I** in the LIF spectrum. The species associated with bands **A-D**, show a pair of the OH stretching bands of the bidentate hydrogen-bonding, indicating different isomers of B18C6-$(H_2O)_1$. Species **E, F and G** are due to B18C6-$(H_2O)_2$ complexes. The IR spectra of **E** and **G** show that each of two water molecules forms bidentate hydrogen-bonding to B18C6, while the species **F** shows the

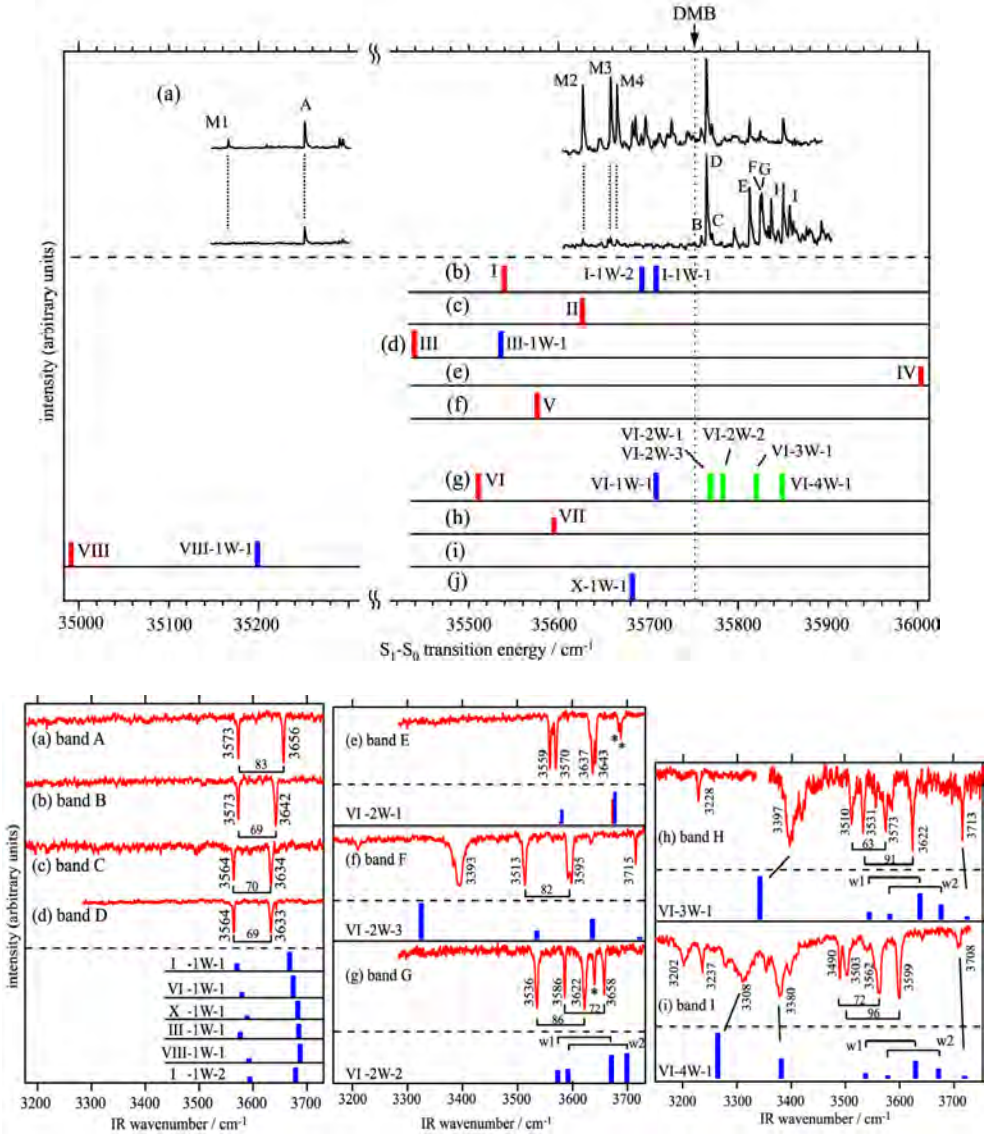

Fig. 19. (Upper) (a) LIF spectra of jet-cooled B18C6 and its hydrated complexes obtained without and with adding water vapor. (b-j) TD-DFT calculated S_1-S_0 transition energies of the structures given in Figure 20. The red, blue, and green bars correspond to bare B18C6, B18C6-$(H_2O)_1$, and B18C6-$(H_2O)_{2\text{-}4}$, respectively. (Lower) IR-UV DR spectra (red) of the obtained by monitoring the bands in the LIF spectrum. Also shown are the calculated IR spectra (blue) of the structures given in Figure 20. Figure adapted from Ref. (Kusaka et al., 2009).

IR spectrum similar to that of species **c** of DB18C6-$(H_2O)_2$, Figure 18. The IR spectra of higher size complexes, **H** and **D**, exhibits the two pair of OH stretching bands associate with the bidentate hydrogen-bonding. Species **A** and species **B-D** can be assigned to isomers of B18C6-$(H_2O)_1$ built on **M1** and **M2-M4**, respectively from the similar values of blue-shifts (~100 cm-1) of the complexes. Interestingly, the intensity of band **D** is strongest among the isomers of B18C6-$(H_2O)_1$, which means that species **D** has the structure preferred for the complex formation with the water molecule. Bands **E-I** are assigned to larger hydrated complexes built based on species **D**.

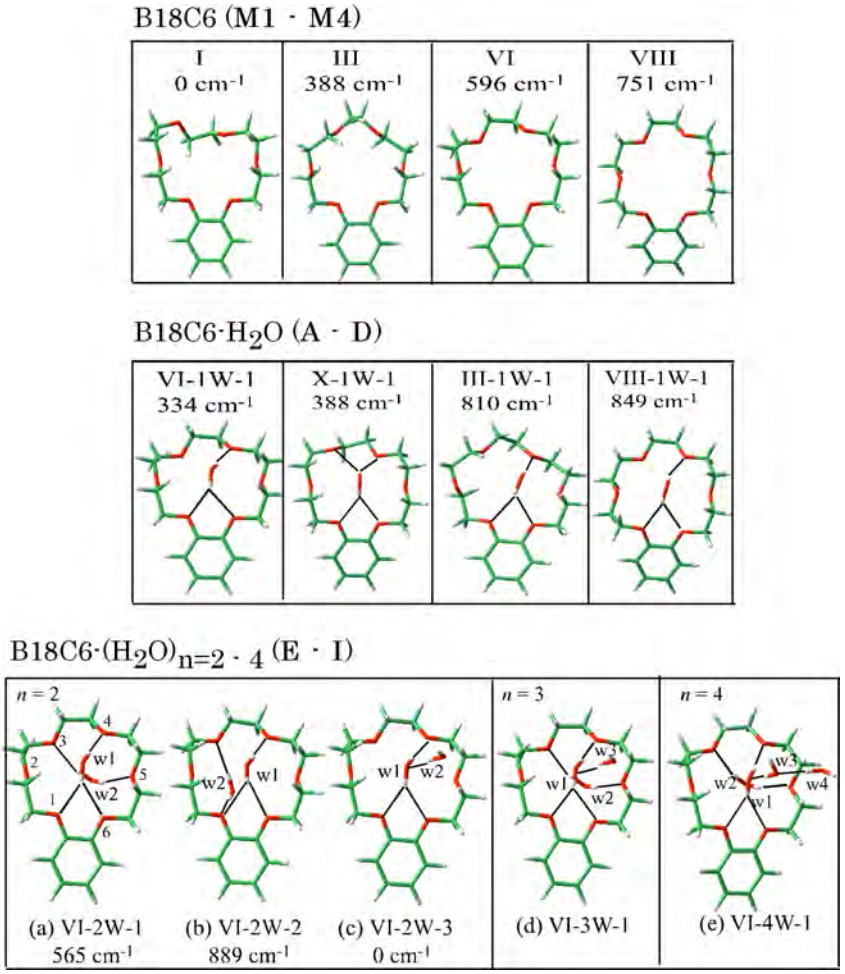

Fig. 20. (Upper) Most probable structures of B18C6 and B18C6-$(H_2O)_1$. All the calculations are done at B3LYP/6-31+G* level. (Lower) Probable structures of (a-c) B18C6-$(H_2O)_2$, (d) B18C6-$(H_2O)_3$, and (e) B18C6-$(H_2O)_4$ at the B3LYP/6-31+G* level. The numbers shown in cm^{-1} represent the electronic energies of the isomers relative to that of VI-2W-3. Solid and dotted lines show H-bonding from the front and back sides of B18C6, respectively. Figure adapted from Ref. (Kusaka et al., 2009).

The determination of the structures of bare B18C6 and B18C6-$(H_2O)_1$ is not so straight forward, because of larger number of possible conformers and isomers than those of DB1816. In the calculation, we obtained eight lowest energy conformers for bare B18C6 within the energy of 800 cm^{-1} at B3LYP/6-31+G* level. The IR spectra in the CH stretching region were not helpful. Instead, we determined the structures by two steps; (1) we first examined whether each conformer has the structure which can incorporate H_2O by the bidentate H-bonding. (2) we then compared the TD-DFT calculated electronic transition energy with the observed transition. Figure 20 shows the possible structures for **M1-M4** and **A-D**. Among the B18C6-$(H_2O)_1$ complexes of **A-D**, the intensity of species **D** is strongest, meaning this species with the structure of VI or X is the preferred geometry for the encapsulation of H_2O. We also see that larger size B18C6-$(H_2O)_n$ complexes are grown based on this structure, Figure. 21. It is not clear why B18C6 prefers the conformer VI or X, upon the complex formation with water because neither conformer VI nor X is the most stable structure at the B3LYP/6-31+G* level calculation. However, since the energy differences for different conformers are very small and it is quite possible that higher level of calculation will give more reliable energies. Anyway, similar to the case of DB18C6, there is a preferred structure of B18C6 to incorporate water molecule(s), which is strongly related to the molecular recognition of the host/guest complexes.

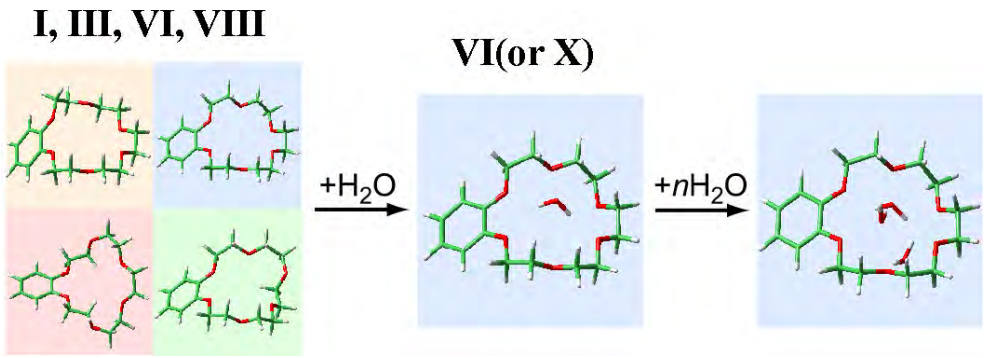

Fig. 21. Conformer preference for the formation of B18C6-$(H_2O)_n$ host-guest complexes. Figure adapted from Ref. (Kusaka et al., 2009).

7. Conclusion

In this chapter, we described our combined study of laser spectroscopic work and theoretical calculation for the determination of the structures of gas phase amino acids and host/guest complexes cooled in supersonic jets. The cooling effect of the supersonic jets enabled to simplify the electronic spectra of those molecules and complexes which are difficult in condensed phase. The double resonance spectroscopic technique, UV-UV hole-burning and IR-UV double resonance, is quite powerful to discriminate difference species including conformers and isomers and to measure the IR spectrum of individual species. For amino acids, it was found that different conformers have different fluorescence lifetimes though its reason is not clear. Also it was found that water molecules prefer the open conformers for the hydration. For the encapsulation complex of calix[4]arene, we showed that it can encapsulate variety of guest species in its cavity by use of difference interaction

depending on the guest. In the crown ether systems, a conformer change and preference were observed for forming the inclusion complexes for specific guests. These are the simplest examples of the molecular recognition of the host-guest complex. In near future, this study will be extended to much larger molecular systems by developing the technique of vaporization of nonvolatile large molecule, such as using laser ablation and electro-spray.

8. References

Anderson, J. D.; Paulsen, E. S. & Dearden, D. (2003). Alkali metal binding energies of dibenzo-18-crown-6: experimental and computational results. *International Journal of Mass Spectrometry,* Vol.227, No.1 pp. 63-76, ISSN 1387-3806

Armentrout, P. B. (1999). Cation–ether complexes in the gas phase: thermodynamic insight into molecular recognition. *International Journal of Mass Spectrometry,* Vol.193, No.2-3 pp. 227-240, ISSN 1387-3806

Atwood, J. L.; Hamada, F.; Robinson, K. D.; Orr, G. W. & Vincent, R. L. (1991). X-ray diffraction evidence for aromatic π hydrogen bonding to water. *Nature,* Vol.349, No.6311, pp. 683-684, ISSN 0028-0836

Atwood, J.L.; Barbour L. J. & Jerga A. (2002) Organization of the interior of molecular capsules by hydrogen bonding. *Proceedings of the National Academy of Sciences,* Vol.99, No.8, pp. 4837-4841, ISSN 0027-8424

Benevelli, F.; Kolodziejski, W.; Wozniak, K. & Klinowski, J. (1999). Solid-state NMR studies of alkali metal ion complexes of *p*-tertbutyl-calixarenes. *Chemical Physics Letters,* Vol.308, No.1-2, pp. 65-70, ISSN 0009-2614

Brocos P.; Banquy X.; Díaz-Vergara N.; Pérez-Casas S.; Costas M. & Piñeiro Á. (2010). Similarities and Differences Between Cyclodextrin−Sodium Dodecyl Sulfate Host−Guest Complexes of Different Stoichiometries: Molecular Dynamics Simulations at Several Temperatures. *The Journal of Physical Chemistry B,* Vol.114, No.39, pp. 12455-12467, ISSN 1089-5647

Brutschy, B. (2000). The Structure of Microsolvated Benzene Derivatives and the Role of Aromatic Substituents. *Chemical Reviews,* Vol.100, No.11 pp. 3891-3920, ISSN 0009-2665

Dunning, T. H., Jr. (1989). Gaussian basis sets for use in correlated molecular calculations. I. The atoms boron through neon and hydrogen. *Journal of Chemical Physics,* Vol.90, No.2 pp. 1007-1989, ISSN 0021-9606

Ebata, T. (1998). Population Labelling Spectroscopy, In: *Nonlinear Spectroscopy for Molecular Structure Determination,* Field, R. W., Hirota E., Maier J. P., Tsuchiya, S., (pp. 149-165), Blackwell Science, ISBN 0-632-04217-6, Oxford

Ebata, T.; Fujii, A. & Mikami, N. (1998). Vibrational spectroscopy of small-sized hydrogen-bonded clusters and their ions. *International Reviews in Physical Chemistry,* Vol.17, No.4, pp. 331-361, ISSN 0144-235X

Ebata, T. ; Hashimoto, T.; Ito, T. ; Inokuchi, Y. ; Altunsu, F. ; Brutschy, B. & Tarakeshwar, P. (2006). Hydration profiles of aromatic amino acids: conformations and vibrations of L-phenylalanine–$(H_2O)_n$ clusters. *Physical Chemistry Chemical Physics,* Vol.8, No.41, pp. 4783-4791, ISSN 1463-9076

Ebata, T.; Hodono, Y.; Ito, T. & Inokuchi, Y. (2007). Electronic spectra of jet-cooled calix[4]arene and its van der Waals clusters: Encapsulation of a neutral atom in a molecular bowl. *Journal of Chemical Physics,* Vol.126, No.14 pp. 141101-1-14101-4, ISSN 0021-9606

Ebata, T. (2009). Study on the Structure and Vibrational Dynamics of Functional Molecules and Molecular Clusters by Double Resonance Vibrational Spectroscopy. *Bulletin of the Chemical Society of Japan,* Vol.82, No.2, pp. 127-151, ISSN 0009-2673

Ebata, T.; Hontama, N.; Inokuchi, Y.; Haino, T.; Apra, E. & Xantheas, S. S. (2010). Encapsulation of Ar_n complexes by calix[4]arene: *endo- vs. exo*-complexes. *Physical Chemistry Chemical Physics,* Vol.12, No.18, pp. 4569-4579, ISSN 1463-9076

Frisch, M. J.; Trucks, G. W.; Schlegel, H. B.; Scuseria, G. E.; Robb, M. A.; Cheeseman, J. R.; Scalmani, G.; Barone, V.; Mennucci, B.; Petersson, G. A.; Nakatsuji, H.; Caricato, M.; Li, X.; Hratchian, H. P.; Izmaylov, A. F.; Bloino, J.; Zheng, G.; Sonnenberg, J. L.; Hada, M.; Ehara, M.; Toyota, K.; Fukuda, R.; Hasegawa, J.; Ishida, M.; Nakajima, T.; Honda, Y.; Kitao, O.; Nakai, H.; Vreven, T.; Montgomery, J. A., Jr.; Peralta, J. E.; Ogliaro, F.; Bearpark, M.; Heyd, J. J.; Brothers, E.; Kudin, K. N.; Staroverov, V. N.; Kobayashi, R.; Normand, J.; Raghavachari, K.; Rendell, A.; Burant, J. C.; Iyengar, S. S.; Tomasi, J.; Cossi, M.; Rega, N.; Millam, J. M.; Klene, M.; Knox, J. E.; Cross, J. B.; Bakken, V.; Adamo, C.; Jaramillo, J.; Gomperts, R.; Stratmann, R. E.; Yazyev, O.; Austin, A. J.; Cammi, R.; Pomelli, C.; Ochterski, J. W.; Martin, R. L.; Morokuma, K.; Zakrzewski, V. G.; Voth, G. A.; Salvador, P.; Dannenberg, J. J.; Dapprich, S.; Daniels, A. D.; Farkas, O.; Foresman, J. B.; Ortiz, J. V.; Cioslowski, J. & Fox, D. J. (2009). Gaussian 09, revision A.02; Gaussian, Inc.: Wallingford, CT

Glendening, E. D.; Feller, D. & Thompson, M. A. (1994). An Ab Initio Investigation of the Structure and Alkali Metal Cation Selectivity of 18-Crown-6. *Journal of the American Chemical Society,* Vol.116, No.23, pp. 10657-10669, ISSN 0002-7863

Gokel, G. W. (1991). *Crown Ethers and Cryptands.* Royal Society of Chemistry, ISBN 0-85186-996-3, Cambridge, UK.

Gutsche, C. D. (1998) *Calixarenes revisited: Monographs in Supramolecular Chemistry*, Royal Society of Chemistry, ISBN 978-0854045020, Cambridge, UK.

Hashimoto, T. ; Takasu, Y. ; Yamada, Y. & Ebata, T. (2006). Anomalous conformer dependent S_1 lifetime of L-phenylalanine. *Chemical Physics Letters,* Vol.421, No.1-3, pp. 227-231, ISSN 0009-2614

Hontama N.; Inokuchi Y.; Ebata T.; Dedonder-Lardeux C.; Jouvet C. & Xantheas S. S. (2010). Structure of the Calix[4]arene−(H_2O) Cluster: The World's Smallest Cup of Water. *The Journal of Physical Chemistry A,* Vol.114, No.9, pp. 2967-2972, ISSN 1089-5639

Inokuchi, Y. ; Kobayashi, Y.; Ito, T. & Ebata, T. (2007). Conformation of L-Tyrosine Studied by Fluorescence-Detected UV−UV and IR−UV Double-Resonance Spectroscopy. *The Journal of Physical Chemistry A,* Vol.111, No.17, pp. 3209-3215, ISSN 1089-5639

Inokuchi, Y.; Boyarkin, O. V.; Kusaka, R. ; Haino, T. ; Ebata, T.& Rizzo, T.R. (2011). UV and IR spectroscopic Studies of Cold Alkali Metal Ion-Crown Ether Complexes in the Gas Phase. *Journal of the American Chemical Society,* Vol.133, No.31, pp. 12256-12263, ISSN 0002-7863

Izatt, R. M.; Rytting, J. H.; Nelson, D. P.; Haymore, B. L. & Christensen, J. J. (1969). Binding of Alkali Metal Ions by Cyclic Polyethers: Significance in Ion Transport Processes. *Science,* Vol.164, No.3878, pp. 443-444, ISSN 0036-8075

Kaneko, S., Inokuchi, Y., Takayuki Ebata, T.; Aprà E. & Xantheas, S. S. (2011). Laser Spectroscopic and Theoretical Studies of Encapsulation Complexes of Calix[4]arene. *The Journal of Physical Chemistry A,* Vol.115, No.40, pp. 10846-10853, ISSN 1089-5639

Kendall, R.; Dunning, T., Jr. & Harrison, R. (1992). Electron affinities of the first-row atoms revisited. Systematic basis sets and wave functions. *Journal of Chemical Physics,* Vol.96, No.9 pp. 6796-6806, ISSN 0021-9606

Kusaka, R. ; Inokuchi, Y. & Ebata, T. (2007). Laser spectroscopic study on the conformations and the hydrated structures of benzo-18-crown-6-ether and dibenzo-18-crown-6-ether in supersonic jets. *Physical Chemistry Chemical Physics,* Vol.9, No.32, pp. 4452-4459, ISSN 1463-9076

Kusaka, R. ; Inokuchi, Y. & Ebata, T. (2008). Structure of hydrated clusters of dibenzo-18-crown-6-ether in a supersonic jet—encapsulation of water molecules in the crown cavity. *Physical Chemistry Chemical Physics,* Vol.10, No.41, pp. 6238-6244, ISSN 1463-9076

Kusaka, R. ; Inokuchi, Y. & Ebata, T. (2009). Water-mediated conformer optimization in benzo-18-crown-6-ether/water system. *Physical Chemistry Chemical Physics,* Vol.11, No.40, pp. 9132-9140, ISSN 1463-9076

Kusaka, R.; Kokubu, S.; Inokuchi, Y.; Haino, T. & Ebata, T. (2011). Structure of host-guest complexes between dibenzo-18-crown-6 and water, ammonia, methanol, and acetylene: Evidence of molecular recognition on the complexation. *Physical Chemistry Chemical Physics,* Vol.13, No.15, pp. 6827-6836, ISSN 1463-9076

Kuzmicz, R.; Dobrzycki, L.;Wozniak, K.; Benevelli, F.; Klinowski, J. & Kolodziejski, W. (2002). X-ray diffraction and ^{13}C solid-state NMR studies of the solvate of tetra(C-undecyl)calix[4]resorcinarene with dimethylacetamide. *Physical Chemistry Chemical Physics,* Vol.4, No.11, pp. 2387-2391, ISSN 1463-9076

Lee, K. T; Sung, J.; Lee, K. J. & Kim, S. K. (2002). Resonant two-photon ionization study of jet-cooled amino acid: L-phenylalanine and its monohydrated complex. *Journal of Chemical Physics,* Vol.116, No.19 pp. 8251-8254, ISSN 0021-9606

Lehn, J. -M. (1995). *Supramolecular Chemistry: Concepts and Perspectives,* Wiley-VCH, ISBN 978-3527293117, Weinheim, Germany

Lide, R. D. (2001). *CRC Handbook of Chemistry and Physics* (82nd Ed.), CRC Press, pp. 9-45, ISBN 978-0849304828

Molins, M. A.; Nieto, P. M.; Sanchez, C.; Prados, P.; Mendoza, J. De. & Pons, M. (1992). Solution structure and conformational equilibria of a symmetrical calix[6]arene. Complete sequential and cyclostereospecific assignment of the low-temperature

NMR spectra of a cycloasymmetric molecule. *The Journal of Organic Chemistry,* Vol.57, No.25, pp. 6924-6931, ISSN 0022-3263

More, M. B.; Ray, D. & Armentrout, P. D. (1999). Intrinsic Affinities of Alkali Cations for 15-Crown-5 and 18-Crown-6: Bond Dissociation Energies of Gas-Phase M^+−Crown Ether Complexes. *Journal of the American Chemical Society,* Vol.121, No.2, pp. 417-423, ISSN 0002-7863

Møller, C. & Plesset, M. S. (1934). Note on an Approximation Treatment for Many-Electron Systems. *Physical Review,* Vol.46, No.7 pp. 618-622, ISSN 0031-899X

Pedersen, C. J. (1967). Cyclic polyethers and their complexes with metal salts. *Journal of the American Chemical Society,* Vol.89, No.26, pp. 7017-7036, ISSN 0002-7863

Pedersen, C. J. & Frensdorff, H. K. (1972). Macrocyclic Polyethers and Their Complexes. *Angewandte Chemie International Edition,* Vol.11, No.1, pp. 16-25, ISSN 0570-0833

Peiris, D. M.; Yang, Y.; Ramanathan, R.; Williams, K. R.; Watson, C. & Eyler, J. R. (1996). Infrared multiphoton dissociation of electrosprayed crown ether complexes. *International Journal of Mass Spectrometry and Ion Processes,* Vol.157-158, pp. 365-378, ISSN 0020-7381

Purse, B.W.; Gissot, A. & Rebek, J. Jr (2005). A Deep Cavitand Provides a Structured Environment for the Menschutkin Reaction. *Journal of the American Chemical Society,* Vol.127, No.32, pp. 11222-11223, ISSN 0002-7863

Robertson, E. & Simons, J. P. (2001). Getting into shape: Conformational and supramolecular landscapes in small biomolecules and their hydrated clusters. *Physical Chemistry Chemical Physics,* Vol.3, No.1, pp. 1-18, ISSN 1463-9076

Snoek, L. C.; Robertson, E. G.; Kroemer, R. T. & Simons, J. P. (2000). Conformational landscapes in amino acids: infrared and ultraviolet ion-dip spectroscopy of phenylalanine in the gas phase. *Chemical Physics Letters,* Vol.321, No.1-2, pp. 49-56, ISSN 0009-2614

Szejtli, J (1988). *Cyclodextrin Technology: Topics in Inclusion Science,* Springer, ISBN 978-9027723147, Dordrecht, The Netherlands

Tanabe, S.; Ebata, T.; Fujii, M. & Mikami, N. (1993). OH stretching vibrations of phenol—$(H_2O)_n$ (n=1–3) complexes observed by IR-UV double-resonance spectroscopy. *Chemical Physics Letters,* Vol.215, No.4, pp. 347-352, ISSN 0009-2614

Thallapally, P. K.; Lloyd, G. O.; Atwood ,J. L. & Barbour , L.J. (2005) Diffusion of Water in a Nonporous Hydrophobic Crystal. *Angewandte Chemie International Edition,* Vol.44, No.25 , pp. 3848-3851, ISSN 0570-0833

Von Helden, G. ; Compagnon, I.; Blom, M. N.; Frankowski, M. ; Erlekam, U. ; Oomens, J.; Brauer, B. ; Gerber, R. B. & Meijer, G. (2008). Mid-IRspectra of different conformers of phenylalanine in the gas phase. *Physical Chemistry Chemical Physics,* Vol.10, No.9, pp. 1248-1256, ISSN 1463-9076

Watanabe, T. ; Ebata, T.; Tanabe S. & Mikami, N. (1996). Size-selected vibrational spectra of phenol-$(H_2O)_n$ (n=1–4) clusters observed by IR–UV double resonance and stimulated Raman-UV double resonance spectroscopies. *Journal of Chemical Physics,* Vol.105, No.2 pp. 408-419, ISSN 0021-9606

Zwier, T. S. (1996). THE SPECTROSCOPY OF SOLVATION IN HYDROGEN-BONDED AROMATIC CLUSTERS. *Annual Review of Physical Chemistry,* Vol.47, pp. 205-241, ISSN 0066-426X